

Gyrokinetic simulations with external resonant magnetic perturbations: Island torque and nonambipolar transport with plasma rotation

R. E. Waltz^{1,a)} and F. L. Waelbroeck²

¹General Atomics, P.O. Box 85608, San Diego, California 92186-5608, USA

²Institute of Fusion Studies, University of Texas, Austin, Texas 78712, USA

(Received 11 October 2011; accepted 7 February 2012; published online 23 March 2012)

Static external resonant magnetic field perturbations (RMPs) have been added to the gyrokinetic code GYRO [J. Candy and R. E. Waltz, *J. Comp. Phys.* **186**, 545 (2003)]. This allows nonlinear gyrokinetic simulations of the nonambipolar radial current flow j_r , and the corresponding $\vec{j} \times \vec{B}$ plasma torque (density) $R[j_r B_p/c]$, induced by magnetic islands that break the toroidal symmetry of a tokamak. This extends the previous GYRO formulation for the transport of toroidal angular momentum (TAM) [R. E. Waltz, G. M. Staebler, J. Candy, and F. L. Hinton, *Phys. Plasmas* **14**, 122507 (2007); errata **16**, 079902 (2009)]. The focus is on electrostatic full torus radial slice simulations of externally induced $q = m/n = 6/3$ islands with widths 5% of the minor radius or about 20 ion gyroradii. Up to moderately strong $E \times B$ rotation, the island torque scales with the radial electric field at the resonant surface E_r , the island width w , and the intensity I of the high- n micro-turbulence, as $E_r w \sqrt{I}$. The radial current inside the island is carried (entirely in the $n = 3$ component) and almost entirely by the ion $E \times B$ flux, since the electron $E \times B$ and magnetic flutter particle fluxes are cancelled. The net island torque is null at zero E_r rather than at zero toroidal rotation. This means that while the expected magnetic braking of the toroidal plasma rotation occurs at strong co- and counter-current rotation, at null toroidal rotation, there is a small co-directed magnetic acceleration up to the small diamagnetic (ion pressure gradient driven) co-rotation corresponding to the zero E_r and null torque. This could be called the residual stress from an externally induced island. At zero E_r , the only effect is the expected partial flattening of the electron temperature gradient within the island. Finite-beta GYRO simulations demonstrate almost complete RMP field screening and $n = 3$ mode unlocking at strong E_r . © 2012 American Institute of Physics. [<http://dx.doi.org/10.1063/1.3692222>]

I. INTRODUCTION AND SUMMARY

Static external resonant magnetic perturbations (RMPs) have been added to the δf -gyrokinetic code GYRO.¹ This allows nonlinear gyrokinetic simulations of the nonambipolar radial current flow j_r , and the corresponding $\vec{j} \times \vec{B}$ plasma torque (density) $-R[j_r B_\theta/c]$, induced by magnetic islands that break the toroidal ϕ -symmetry of a tokamak. At large toroidal rotation, the externally induced island torque is said to “brake” the rotation. This paper extends the previous GYRO formulation for the transport of toroidal angular momentum (TAM) (Ref. 2) and explores a novel *island residual stress* from externally induced islands at very low diamagnetic level toroidal rotation. The initial focus is on collisionless electrostatic (zero beta) full (and partial) torus radial slice turbulent transport simulations with externally induced $q = m/n = 6/3$ island with a width of about 5% of the plasma radius or about 20 ion gyroradii in toroidally rotating tokamak plasmas.

It is well known³ that magnetic islands resulting from spontaneous growth of tearing modes in the core can degrade plasma energy confinement if large enough, but externally controlled multiple helicity RMPs have been found to control the so-called edge localized modes (ELMs) without

degrading the H-mode pedestal pressure.⁴ These vacuum RMP fields appear to induce overlapping islands with stochastic field lines at the edge. This paper is not so ambitious as to treat this rich edge RMP phenomenology, but rather focuses on the simpler problem of a stationary externally induced single helicity low- n island embedded in a high level of high- n gyrokinetic turbulence with (and without) a high level of core plasma rotation.

It is generally well known that the particle transport in toroidally symmetric magnetic fields is *intrinsically ambipolar* with ions and electrons radially transporting equally independent of the radial electric field, whereas broken toroidal symmetry (as from an externally induced island) is said to induce a (transient) *nonambipolar* radial current dependent on the (instantaneous) radial electric field.⁵ However, little has been written quantifying the strength of this dependence or even its form for an externally induced island in the presence of strong turbulent transport. An often used heuristic model of nonambipolar transport assumes $j_r = ZeD[-\partial n/\partial r + (Zen/T)E_r]$, where the least confined species (the one with the largest cross field effective diffusion D) is said to carry the radial current flux which ceases when that species has a Boltzmann (or adiabatic) distribution: $\partial n/\partial r = -(Zen/T)\partial\phi/\partial r$.⁶ If the ions ($Z = 1$) drifting across the field lines of the island are the least confined species, then the heuristic formula suggests the radial current flux and

^{a)}Electronic mail: waltz@fusion.gat.com.

braking torque should be proportional to the toroidal velocity v_ϕ : $j_r \propto v_\phi = c/B_0[E_r - (T_i/en)\partial n/\partial r]$ (ignoring temperature gradients and neoclassical poloidal rotation). With the externally induced island stationary, the radial current and torque vanish when the ions are at rest $v_\phi = 0$; this can be called the “ion root.” On the other hand, since the electrons ($Z = -1$) traveling parallel to the field around the island are most likely to be the least radially confined, the heuristic formula suggests that the radial current and torque vanish when the electrons are tied to the field lines with their $E \times B$ motion cancelling their diamagnetic motion; this could be called as the “electron root.” The latter actually implies that an external RMP island acting on the plasma with the local ion center of mass at rest ($v_\phi = 0$) would accelerate the plasma (local to the island) to a co-current low (diamagnetic) toroidal rotation $v_\phi = c/B_0\{-(T_e + T_i/en)\partial n/\partial r\}$ (again ignoring temperature gradients), i.e., there could be an *island residual stress* giving spontaneous co-rotation (without another source of TAM).

For the turbulently driven RMP single helicity island torque demonstrated in this paper, the *nonambipolar* radial current peaks on the (unperturbed) resonant singular flux surface and is supported only over the island width. Somewhat paradoxically in light of the heuristic model above, even though the electrons are the dominant (controlling) species, the ions carry (essentially) all the radial current. The simulations (in Sec. IV) show that the magnetic radial current flux of electrons ($\delta j_{\parallel}^e \Delta B_r^{ext}/B$) is canceled by the $E \times B$ electron radial current flux ($\Delta v_r^E \delta \rho^e$), where a *helical* $E \times B$ electric potential $\Delta \phi$ is induced by the RMP field (ΔB_r^{ext}) to “hold back” the induced island parallel field current δj_{\parallel}^e perturbation (δj_{\parallel}^i is very small). Since the $E \times B$ particle flux is *intrinsically ambipolar* (from charge quasineutrality) $\delta \rho^i = -\delta \rho^e$, the $E \times B$ radial ion transport ($\Delta v_r^E \delta \rho^i$) can be said to exclusively carry the radial current. Alternatively since the $E \times B$ currents cancel, the magnetic electron radial transport can be said to exclusively carry the current: $\delta j_{\parallel}^e \Delta B_r^{ext}/B = \Delta v_r^E \delta \rho^i$.

A better heuristic model for the peak island electron radial current is $j_r^e = -e[-D^{ExB}\partial n/\partial r + n\mu^M E_r]$ with the electron radial mobility $\mu^M < 0$ reflecting the strong parallel field mobility $\Delta j_{\parallel}^e = -eD_{\parallel}[-\nabla_{\parallel}\Delta n + n(e/T)\nabla_{\parallel}\Delta\phi]$, where $\mu_{\parallel} = (-e/T)D_{\parallel}$. [The distortions within the island Δn , $\Delta\phi$ (as well as ΔT_e , ΔT_i) are illustrated in Sec. III, where it is shown that $\Delta E_r = -\partial\Delta\phi/\partial r$ partially cancels the imposed E_r and Δn roughly tracks $n(e/T)\Delta\phi$ keeping the electron close to adiabatic in the parallel field direction.] The ions having negligible mobility along field lines ($\mu^M \sim 0$) have $j_r^i = e[-D^{ExB}\partial n/\partial r]$. The net result is that the total peak island radial current is best described by $j_r = -e[\mu^M n]E_r = e[-D^{ExB}\partial n/\partial r] = j_r^i$, i.e., the ions carry all the current (as discussed in Sec. IV). A key result is that the null torque is obtained at $E_r \sim 0$, which means there is an *island residual stress* spontaneously accelerating the ions (local to the island) in the co-current direction to $v_\phi = -c/B_p[\partial P^i/\partial r]/en$ (when both density and temperature gradients are included but temperature gradient driven neoclassical poloidal rotation is ignored). In essence, this paper describes how the island radial conductivity $\sigma_r = -e^2 n \mu^M > 0$

scales with the strengths of the high- n turbulence and the RMP field. At $E_r \sim 0$, the only significant effect of the island is the expected electron temperature gradient flattening inside and steepening outside the island which signals the loss of energy confinement within the island. The increase or decrease of the unperturbed flux surface average density and potential gradients depends on the sign of E_r .

We hasten to remind that (even with toroidal axisymmetry) TAM transport at low toroidal rotation has many sources of *residual stress* from diamagnetic level velocity shears.⁷ In addition, the GYRO turbulent RMP island simulations here (or in Ref. 7) do not explicitly contain any neoclassical flows or effects such as the neoclassical toroidal viscosity (NTV) torque⁸ which drives toward a diamagnetic level counter-current toroidal flow proportional to the ion temperature gradient when axisymmetry is broken *non-resonantly* (analogous to the well known neoclassical poloidal flow from broken toroidal symmetry).

The high- n ion temperature gradient (ITG) and trapped electron mode (TEM) micro-turbulence nonlinearly pump the island nonambipolar radial current which is carried exclusively in the RMP toroidal mode number ($n = 3$ in our case). As we discuss in Sec. IV, the peak island radial current is independent of ΔB_r^{ext} , but the radially integrated island torque density (island radial current induced TAM flux or Maxwell stress) scales with island width $w \propto \sqrt{\Delta B_r^{ext}}$, instantaneous and local radial electric field E_r , and high- n turbulence intensity I as $\Pi^{ext} \propto w E_r \sqrt{I}$. External to the island, the external RMP field appears to nonlinearly pump the zonal flows and reduce the background driving ion temperature gradients to an extent; this in turn reduces the background energy and (viscous or Reynolds stress) momentum transport flux to an extent. [We interpret this as an artifact of the simulation boundary conditions and that transport fluxes (with and without an island) should only be compared at the same background driving gradients.] Of course starting from a high rotation with large E_r , the island nonambipolar current flux cannot last long; the net island torque rather quickly “brakes” the toroidal rotation and, from radial force, remaining E_r (near the island) falls presumably to zero (as does the radial current according to $j_r = -e[\mu^M n]E_r = e[-D^{ExB}\partial n/\partial r] = j_r^i$), if only this process is considered and there is no added source of TAM.

The electrostatic turbulent RMP island braking process (just described) is greatly complicated at finite-beta. When the plasma is rotating, diamagnetic plasma currents build up an opposing “screening” magnetic field δB_r of the same mode number and helicity but somewhat out of (anti-) phase with the RMP field ΔB_r^{ext} . Our simulations (in Sec. V) show that for small E_r , the island shifts in the direction of rotation flow as a result of the viscous entrainment with the surrounding plasma. The shift in the relative phase between the island and the driving RMP field causes the island to shrink from its “vacuum” width w (discussed above). As the background E_r increases, a threshold is reached such that the electromagnetic forces exerted by the RMP on the island can no longer balance the turbulent viscous force from the surrounding plasma. The simulations show that the island suddenly “unlocks” and co-rotates with the surrounding plasma. The

rotating island experiences a vanishing drive from the fixed (in the lab frame) RMP field; the island “heals” leaving behind a screened island of very small width. The penetration of a static error (or RMP) field and its dependence on plasma rotation was first treated in the pioneering work of Fitzpatrick^{9,10} in the context of resistive MHD and later with a non-turbulent collisional two fluid model.¹¹ The dynamic screening and mode locking (unlocking) processes in a rotating plasma is quite complicated with bifurcated states and hysteresis possible. It is further complicated by interaction with slow growing intrinsic (Δ' driven) and neoclassical tearing modes (NTMs) (neither treated here). This and other previous works on the theory and observation of magnetic islands have been recently reviewed by Waelbroeck.³

The treatment of a static externally induced island embedded in gyrokinetic turbulence is not without precedent: simulations with the full-f ORB5 (Ref. 12) and the delta-f GKW (Ref. 13) gyrokinetic codes have been published. Both treatments were electrostatic and focused only on heat flux through the island and flattening within the island of the radial temperature gradients (and distortion of the density profile¹³ through both the X- and O- points. In particular, Ref. 13 notes a potential vortex within the island with an apparent “anti-correlation between the radial heat flux generated by the vortex and the ‘magnetic flutter,’ i.e., the heat flux due to the motion along the perturbed magnetic field that forms the island;” this “anti-correlation” is clearly related to the cancellation effects in the nonambipolar radial current flux in our simulation (as discussed above). Both papers have the background $E_r = 0$ and neither treats nonambipolar island radial current and torque with respect to plasma rotation. The closest reference on turbulent islands with plasma rotation is the work of Waelbroeck *et al.*,¹⁴ which presented slab simulations with an electrostatic cold ion collisional drift wave model generalized to include a static island. We provide a detailed comparison to this work in Sec. IV.

The knowledgeable reader may wish to skip over Sec. II of the paper. Section II formulates the extension of the GYRO gyrokinetic equation to include an external RMP field and the subtle details needed to interpret the $\vec{j} \times \vec{B}$ torque density in the TAM transport equation. Transport fluxes from the simulations are given with respect to averages over the *unperturbed* magnetic flux surfaces, and an important distinction is made between *gyrokinetic* and *physical* fluxes. Section III provides full torus $\Delta n = 1$ simulations of the background and $m/n = 6/3$ island transport in the energy, particle, and momentum channels for well studied standard case core plasma parameters with typical $E \times B$ and toroidal velocity shears, with and without large E_r . Island distortions of the radial profile gradients through the island are given as a function of the background E_r . Section IV treats the scaling of island nonambipolar current flux and island torque flux with less expensive partial torus $\Delta n = 3$ simulations (and with irrelevant velocity shears neglected). The dynamic time scales for magnetic braking process are clarified. Section V illustrates finite beta (electromagnetic) simulations of the island unlocking RMP and field screening as a function of E_r . The main conclusions have been given above.

II. FORMULATION OF THE GYROKINETIC EQUATIONS WITH AN EXTERNAL RESONANT MAGNETIC FIELD PERTURBATION

Following Refs. 15 and 16, the GYRO code¹ has the $\partial \delta h / \partial t$ form of the gyrokinetic equation for a species of charge Z and temperature T is

$$\begin{aligned} \partial \delta h / \partial t + \vec{v}_E^0 \cdot \vec{\nabla} \delta h + (v_{\parallel} \nabla_{\parallel} + \vec{v}_d \cdot \vec{\nabla}_{\perp}) \delta g + \delta \vec{v}_{\chi} \cdot \vec{\nabla} \delta g + C[\delta f] \\ = -\delta \vec{v}_{\chi} \cdot \vec{\nabla} F_0, \end{aligned} \quad (1)$$

where the adiabatic part of the perturbed gyro-center distribution function δf is

$$\delta g = \delta h + ZeF_0/T \langle \delta \chi \rangle = \delta f + ZeF_0/T \langle \delta \phi \rangle, \quad (2)$$

where F_0 is the (parallel velocity drifted) background Maxwellian and, ignoring the parallel magnetic field perturbations, $\delta \chi = \langle \delta \phi - v_{\parallel} / c \delta A_{\parallel} \rangle$ is the intrinsic perturbed generalized field potential (including the electrostatic $\delta \phi$ and parallel magnetic vector δA_{\parallel} potentials). $\langle \rangle$ denotes a gyro-average, and $\delta \vec{v}_{\chi} = (c/B) \hat{z} \times \vec{\nabla} \delta \chi$ is the generalized perturbed $E \times B$ velocity with $\vec{v}_E^0 = (c/B) \hat{z} \times \hat{z} E_r^0$ the background $E \times B$ (Doppler) rotation with $E_r^0 = \langle -|\vec{\nabla}_r| \partial \Phi_0 / \partial r \rangle$ the radial electric field ($\hat{z} \times \hat{x} = \hat{y}$, $\hat{r} = \hat{x}$ and $\vec{B} = B \hat{z}$ unperturbed magnetic field). v_{\parallel} is the (total) parallel field velocity, \vec{v}_d is the (perpendicular) grad-B and curvature drift, and C is the collision operator.

To add the effects of a *small* static external resonant magnetic perturbations (RMPs), $\Delta \vec{B}_{\perp}^{ext} / B = (\vec{\nabla}_{\perp} \times \hat{z} \Delta A_{\parallel}^{ext}) / B$; it is convenient to convert Eq. (1) to the $\partial \delta f / \partial t$ form while augmenting $\delta A_{\parallel} \Rightarrow \delta A_{\parallel} + \Delta A_{\parallel}^{ext}$ and correspondingly $\delta \vec{v}_{\chi} \Rightarrow \delta \vec{v}_{\chi} + \Delta \vec{v}_{\chi}$ with $\Delta \chi = \langle -v_{\parallel} / c \Delta A_{\parallel}^{ext} \rangle$ and $\Delta \vec{v}_{\chi} = (c/B) \hat{z} \times \vec{\nabla} \Delta \chi$ while keeping $\partial \Delta A_{\parallel}^{ext} / \partial t = 0$

$$\begin{aligned} \partial [\delta f + ZeF_0/T v_{\parallel} / c \langle \delta A_{\parallel} \rangle] / \partial t \\ + \vec{v}_E^0 \cdot \vec{\nabla} \left[\delta f + ZeF_0/T v_{\parallel} / c \langle \delta A_{\parallel} + \Delta A_{\parallel}^{ext} \rangle \right] \\ + (v_{\parallel} \nabla_{\parallel} + \vec{v}_d \cdot \vec{\nabla}_{\perp}) [\delta f + ZeF_0/T \langle \delta \phi \rangle] \\ + (\delta \vec{v}_{\chi} + \Delta \vec{v}_{\chi}) \cdot \vec{\nabla} [\delta f + ZeF_0/T \langle \delta \phi \rangle] + C[\delta f] \\ = -(\delta \vec{v}_{\chi} + \Delta \vec{v}_{\chi}) \cdot \vec{\nabla} F_0. \end{aligned} \quad (3)$$

Converting back to the $\partial \delta h / \partial t$ form used in GYRO, we have

$$\begin{aligned} \partial [\delta h] / \partial t + \vec{v}_E^0 \cdot \vec{\nabla} [\delta h - ZeF_0/T \Delta \chi] \\ + (v_{\parallel} \nabla_{\parallel} + \vec{v}_d \cdot \vec{\nabla}_{\perp}) \delta g + (\delta \vec{v}_{\chi} + \Delta \vec{v}_{\chi}) \cdot \vec{\nabla} \delta g + C[\delta f] \\ = -(\delta \vec{v}_{\chi} + \Delta \vec{v}_{\chi}) \cdot \vec{\nabla} F_0. \end{aligned} \quad (4)$$

The derivation is entirely equivalent to the usual deflection of the parallel magnetic field direction, $\vec{b} = \vec{b}_0 + \delta \vec{B}_{\perp} / B + \Delta \vec{B}_{\perp}^{ext} / B$, while ignoring any deflection of the perpendicular field direction. It is useful to note that the “omega-star” term on the RHS of Eq. (4) driving the high- n turbulence can be written as [ignoring the parallel (or toroidal) velocity shear (see Appendix A of Ref. 2)]

$$\begin{aligned} -\delta \vec{v}_{\chi} \cdot \vec{\nabla} F_0 \Rightarrow -(c/B) \nabla_y \langle \delta \phi - v_{\parallel} / c \delta A_{\parallel} \rangle |\nabla_r| \\ \times [1/L_n + (w/T - 3/2)/L_T] F_0, \end{aligned} \quad (5)$$

where $1/L_n = -d \ln n / dr$; $1/L_T = -d \ln T / dr$; $w = mv^2/2$. Similarly, the linear $\Delta A_{||}^{ext}$ driving terms [on the RHS and LHS of Eq. (4)] can be combined on the RHS as

$$\begin{aligned} & -\Delta \vec{v}_\chi \cdot \vec{\nabla} F_0 + \vec{v}_E^0 \cdot \vec{\nabla} [Ze F_0 / T \Delta \chi] \Rightarrow \\ & - (c/B) \nabla_y \left\langle -v_{||} / c \Delta A_{||}^{ext} \right\rangle |\nabla r| \\ & \times [1/L_n + (w/T - 3/2)/L_T - (Ze/T) \partial \Phi_0 / \partial r] F_0. \quad (6) \end{aligned}$$

The last term in Eq. (6) is solely responsible for any dependence on E_r^0 . Since $\Delta A_{||}^{ext}$ is produced by currents external to the plasma, it does not explicitly enter the plasma Poisson (quasi-neutrality) or Ampere equations which provide the intrinsic perturbation $[\delta \phi, \delta A_{||}]$ from the time advance of δh in Eq. (4).

The instantaneous flux surface average (FSA) radial transport *gyrokinetic* fluxes of particles and energy result from the velocity moments $\int dv^3 [1, w]$ (and similarly for toroidal angular momentum²) of

$$\begin{aligned} \Gamma_r &= \left\langle |\nabla r| (c/B) \left\{ -\nabla_y \left\langle \delta \phi - v_{||} / c (\delta A_{||} + \Delta A_{||}^{ext}) \right\rangle \right\} \delta g \right\rangle_{fsa} \\ &= \left\langle |\nabla r| [(\delta v_\chi)_x + (\Delta v_\chi)_x] \delta g \right\rangle_{fsa}. \quad (7) \end{aligned}$$

Note this is consistent with the flux surface average (FSA) of the nonlinear term $(\delta \vec{v}_\chi + \Delta \vec{v}_\chi) \cdot \vec{\nabla} \delta g$ in Eq. (5) which can be written as $1/V'(r) \partial [V'(r) \Gamma_r] / \partial r$. The FSA *physical* fluxes are derived from implicitly assuming a “local time (or statistical) average” (over several correlation times) as well as a “local radial average” [(on the scale of a few ion gyro-radial),

$$\begin{aligned} \bar{\Gamma}_r &=] \Gamma_r [\\ &= \left\langle |\nabla r| (c/B) \left\{ -\nabla_y [\delta \phi - v_{||} / c (\delta A_{||} + \Delta A_{||}^{ext})] \right\} \langle \delta g \rangle \right\rangle_{fsa}. \quad (8) \end{aligned}$$

The] [and FSA operation allow the $\langle \delta \phi - v_{||} / c (\delta A_{||} + \Delta A_{||}^{ext}) \delta g \rangle \Rightarrow (\delta \phi - v_{||} / c (\delta A_{||} + \Delta A_{||}^{ext})) \langle \delta g \rangle$ transfer of the gyro-averaging. The *physical* fluxes are then consistent with the *physical* density,

$$\begin{aligned} \delta \bar{n} &= -n_0 (Ze/T) \delta \phi + \int dv^3 \langle \delta g \rangle \\ &= -(Ze/T) \int dv^3 F_0 (\delta \phi - \langle \langle \delta \phi \rangle \rangle) + \int dv^3 \langle \delta f \rangle, \quad (9) \end{aligned}$$

where the gyro-average $\langle \rangle$ is on δg . The first term on the LHS of Eq. (9) is the perturbed polarization density and the second is the perturbed density of gyrocenters with $\int dv^3 \langle \delta f \rangle (\vec{x}) \equiv \int dv^3 \delta f (\vec{x} + \vec{\rho})$, where $\vec{\rho}$ is the gyro-radial containing the gyro-phase angle.

The distinction between *gyrokinetic* [Eq. (7)] and *physical* [Eq. (8)] fluxes is an important one for distinguishing *intrinsically ambipolar* from *nonambipolar* particle flow. The *physical* FSA radial current has two components: an $E \times B$ component

$$\begin{aligned} \bar{j}_r^{ExB} &= \sum_s \left\{ Ze \int dv^3 \langle |\nabla r| (c/B) (-\nabla_y \delta \phi) \langle \delta g \rangle \right\rangle_{fsa} \\ &= \sum_s \left\{ Ze \langle |\nabla r| (\delta v_E)_x \delta \bar{n} \right\rangle_{fsa} \end{aligned} \quad (10)$$

and a magnetic flutter (MF) component

$$\begin{aligned} \bar{j}_r^{MF} &= \sum_s \left\{ Ze \int dv^3 \langle |\nabla r| (c/B) \{ -\nabla_y [-v_{||} / c (\delta A_{||} \right. \\ & \left. + \Delta A_{||}^{ext}) \langle \delta g \rangle \right] \right\rangle_{fsa} = \langle |\nabla r| \delta j_{||} (\delta B_x / B + \Delta B_x^{ext} / B) \rangle_{fsa}, \quad (11) \end{aligned}$$

where $\delta j_{||}$ is the *physical* perturbed (ion and electron) current density along the instantaneous total parallel field direction. (Note that we will stay with the conventional term “magnetic flutter,” which normally refers to the usually turbulent or “fluttering” $\delta A_{||}$ part, even though the $\Delta A_{||}^{ext}$ part is not “fluttering.”) Even in the presence of $\Delta A_{||}^{ext}$, the $E \times B$ particle flux is *intrinsically ambipolar* ($\bar{j}_r^{ExB} = 0$) since the instantaneous local quasineutrality $\sum_s \{ Ze \delta n \}_s = 0$ is imposed in the gyrokinetic code. In contrast to Eq. (10), the *gyrokinetic* $E \times B$ radial current is $\bar{j}_r^{ExB} = \sum_s \{ Ze \int dv^3 \langle |\nabla r| (c/B) (-\nabla_y \langle \delta \phi \rangle \delta g) \rangle_{fsa} \}_s$, which is not zero on radial scales shorter than a few ion gyroradii. (The radial profiles of *gyrokinetic* transport fluxes are given in all plots in later sections where the small short scale deviations from zero in \bar{j}_r^{ExB} are apparent. These small deviations are inward and out polarization currents present even without externally induced islands.) In the absence of $\Delta A_{||}^{ext}$, the *physical* MF particle flow is also approximately *intrinsically ambipolar* ($\bar{j}_r^{MF} \approx 0$) if the high- n micro-turbulence is sufficiently localized (locally correlated) so that the local radial average $[\bar{j}_r^{MF}] = 0$ when $\delta \bar{j}_{||}$ and $\delta B_x = \nabla_y \delta A_{||}$ are derived from Ampere’s law ($-\nabla_\perp^2 \delta A_{||} = 4\pi \delta \bar{j}_{||}$) (see Ref. 17).

In the presence of RMP $\Delta A_{||}^{ext}$, which will typically have a helicity m/n (like 6/3 in our examples) aligned with the helicity of the plasma, there will be an externally induced magnetic island at the $q(r_s) = m/n$ resonant surface r_s breaking the toroidal symmetry. As we shall see in Sec. III, the RMP field drives a *nonambipolar* FSA radial current $\bar{j}_r = \bar{j}_r^{MF}$ peaked at r_s and dependent on the radial electric field at the surface $E_r^0(r_s)$. It is important to say that all FSA radial transport fluxes are with respect to the un-perturbed flux surfaces labeled by r , the midplane minor radius, and not with respect to the island flux surfaces which of course have a separatrix. \bar{j}_r is supported radially between $r_s - W/2 < r < r_s + W/2$ where (in large aspect ratio circular geometry where $|\nabla r|(r, \theta) = 1$) the total island width $W = 4[rq/mq] \cdot (\delta B_r + \Delta B_r^{ext}) / B_\theta$ with $q = rB_\phi / RB_\theta$. In the electrostatic GYRO simulations (Secs. III–V), δB_r and $\delta A_{||}$ are zero, and the island is induced by the vacuum external RMP field. In the electromagnetic finite- β simulations (Sec. VI), a diamagnetically induced $\delta A_{||}$ partially cancels (i.e., screens or shields) the $\Delta A_{||}^{ext}$, shrinking the island width W .

The *nonambipolar* radial current flux from the combined magnetic field perturbations $\Delta \delta A_{||} \equiv \delta A_{||} + \Delta A_{||}^{ext}$ provides a (ϕ -toroidally directed) torque density on the RHS (source side) of the toroidal angular momentum TAM continuity equation (see Eqs. (12) and (13) of Ref. 2),

$$\begin{aligned} & \left\langle R(\delta\bar{j}_r\Delta^\delta B_\theta - \delta\bar{j}_\theta\Delta^\delta B_r)/c \right\rangle_{f_{sa}} \\ &= -\left\langle R(B_\theta/B)(\delta\bar{j}_z\Delta^\delta B_x - \delta\bar{j}_x\Delta^\delta B_z)/c \right\rangle_{f_{sa}} \\ &+ \left\langle R(B_\phi/B)(\delta\bar{j}_x\Delta^\delta B_y - \delta\bar{j}_y\Delta^\delta B_x)/c \right\rangle_{f_{sa}}. \end{aligned} \quad (12)$$

Dropping (as we do) parallel field magnetic perturbations $\Delta^\delta B_z = 0$ the first RHS term of Eq. (12) and using Eqs. (28), (25b), and (25c) of Ref. 2, the second term has a zero local radial average $[\langle R[(B_\phi/B)(\delta\bar{j}_x\nabla_x\Delta^\delta A_z + \delta\bar{j}_y\nabla_y\Delta^\delta A_z)]/c \rangle_{f_{sa}}] = 0$; the torque density from the magnetic perturbations reduces to

$$\left\langle R(\delta\bar{j}_r\Delta^\delta B_\theta - \delta\bar{j}_\theta\Delta^\delta B_r)/c \right\rangle_{f_{sa}} \approx -\left\langle R\bar{j}_r B_\theta \right\rangle_{f_{sa}} / c, \quad (13)$$

where again $\bar{j}_r = \bar{j}_r^{MF}$ is the nonambipolar transport current given by Eq. (11) dependent on the radial electric field E_r^0 . As we show in the next sections, the nonambipolar transport current can be represented by $\bar{j}_r(r) = D^M(r)[e^2 n_0/T_e^0 E_r^0(r_s)] = en_0\mu(r)E_r^0(r_s)$, where $D^M(r) > 0$ is supported over $r_s - w/2 < r < r_s + w/2$. $\mu = De/T_e^0 > 0$ can be called as the island charge mobility and $en_0\mu = \sigma > 0$ as the island radial conductivity. As we discuss below, the minus sign [in Eq. (13)] (and $\sigma > 0$) is crucial for island *magnetic braking* of the toroidal rotation and opposite to the $+R\bar{j}_r^0 B_\theta/c = \bar{j}_r^0 \cdot \vec{\nabla}\psi/c$ torque density from any radial current \bar{j}_r^0 carried in the unperturbed background plasma distribution F_0 [see Eq. (12) and Ref. 2]. (To be clear, \bar{j}_r is carried in $\Delta^\delta F$, where $F = F_0 + \Delta^\delta F$ is the total FSA plasma distribution carrying the total radial current $\bar{j}_r^{tot} = \bar{j}_r^0 + \bar{j}_r$.) The FSA TAM continuity equation is

$$\begin{aligned} \partial\langle mn_0 R u_\phi \rangle_{f_{sa}} / \partial t &= -1/V' \partial(V' \langle R \Pi_{\phi x} |\nabla r| \rangle_{f_{sa}}) / \partial r \\ &+ \langle R\bar{j}_r^0 B_\theta \rangle_{f_{sa}} / c - \langle R\bar{j}_r B_\theta \rangle_{f_{sa}} / c + S_{TAM}, \end{aligned} \quad (14)$$

where $\langle R \Pi_{\phi x} |\nabla r| \rangle_{f_{sa}} = \Pi_i$ (encompassing the R lever arm) is the FSA flux or TAM (including convection of TAM). We take F_0 to be a parallel drifted (or better toroidal drifted) Maxwellian, so it is safe to set $\bar{j}_r^0 = 0$. We denote the radial integral of the island torque density $1/V'(r) \int_0^r V'(r') dr' [\langle R\bar{j}_r B_\theta \rangle_{f_{sa}} / c] = \Pi^{ext}(r)$ as the *island torque flux*. Π^{ext} is sometimes called the Maxwell stress in analogy with the plasma (Reynolds or viscous) stress Π_i carried in the ions. Since Π^{ext} involves a radial integration which subsumes the distinction between *gyrokinetic* \bar{j}_r and *physical* \bar{j}_r , it is a more robust quantity.

At leading order radial force balance, the ion velocity is $\vec{u} = \omega(\psi)R\hat{e}_\phi + K(\psi)\vec{B}$, where we will usually ignore any poloidal rotation $u_\theta = KB_\theta$ to focus on the remaining toroidal rotation $u_\phi = \omega R$ where the toroidal rotation frequency is

$$\begin{aligned} \omega(\psi) &= -c[\partial\Phi_0/\partial\psi + (1/n_0e)\partial P_{0i}/\partial\psi] \\ &\approx \langle c/RB_\theta \rangle_{f_{sa}} [E_r^0 + \langle |\nabla r| \rangle_{f_{sa}} / L_{Pi} / en_{0i}]. \end{aligned} \quad (15)$$

At high co-current rotation, $u_\phi > 0$, $E_r^0 > 0$, and $\bar{j}_r > 0$ for positive island radial mobility; hence, $-\langle R\bar{j}_r B_\theta \rangle_{f_{sa}} / c$ *brakes*

u_ϕ . δf -gyrokinetic codes like GYRO, which separate quasi-steady transport time scales from the turbulent time scales, cannot directly treat the *magnetic braking* dynamically (as it occurs on a time scale somewhat faster than the global transport time scale as we discuss in Sec. IV). The simulation fixed input u_ϕ , E_r^0 , and local time average output \bar{j}_r physically decrease in time during the actual *braking* process. Even though E_r^0 is determined from Eqs. (14) and (15), the ultimate source of E_r^0 is the distribution of the FSA charge density of the plasma ρ_c , which also shifts outward with the \bar{j}_r radial outflow (starting from co-current rotation) in the *braking* process by charge conservation: $\partial\langle \rho_c \rangle / \partial t + 1/V' \partial[V' \bar{j}_r^{tot}] / \partial r = 0$.

Before turning to the simulations, there is a caveat on the use of the high- n approximation on low- n fields in GYRO. GYRO has a field line following the grid, so that the normed n -th toroidal harmonic of the m/n RMP field $\hat{A}_{||n}^{ext}(r) \exp[-in\phi + im\theta]$ is

$$(c_{s0}/c)(eA_{||n}^{ext}/T_{e0}) = \hat{A}_{||n}^{ext}(r, \theta) \exp[-in(\phi - q(r)\theta)], \quad (16)$$

where $\hat{A}_{||n}^{ext}(r, \theta) = \hat{A}_{||n}^{ext}(r) \exp[i(m - nq(r))\theta]$ is the amplitude in the field line following $[r, \theta, n]$ basis (normally called the “ballooning mode” amplitude which is expected to have a weak variation in the poloidal angle θ), $c_{s0} = \sqrt{T_{e0}/m_i}$. In the simple infinite aspect ratio circular geometry (used in the simulations here), the perpendicular field gradient operation $\nabla_y \hat{A}_{||n}^{ext}(r, \theta) = [(inq - \partial_\theta)]/r \hat{A}_{||n}^{ext}(r, \theta)$ in the currently programmed GYRO uses the high- n approximation $\nabla_y \hat{A}_{||n}^{ext}(r, \theta) \Rightarrow inq/r \hat{A}_{||n}^{ext}(r, \theta)$. This may be of some concern except that near the island resonant surface $q(r_s) = m/n$ and the locus of action, $\partial_\theta \hat{A}_{||n}^{ext}(r, \theta) \sim 0$, i.e., the θ dependence is weak.

III. ELECTROSTATIC GYROKINETIC SIMULATIONS OF A FULL TORUS RADIAL SLICE CONTAINING A LARGE EXTERNALLY INDUCED MAGNETIC ISLAND

Here, we present full torus radial slice electrostatic ($\beta_e = 0$, $\delta\hat{A}_{||} = 0$) and collisionless ($\nu_{ei} = 0$) GYRO simulations of the well studied GA standard case (GA-std)^{1,7} with a “flat” plasma profile: $R_0/a = 3$, $r_0/a = 0.5$, $q_0 = 2$, $s = d \ln q / d \ln r = 1$, $a/L_T = 3$, $a/L_n = 1$, $T_i/T_e = 1$, $n_i/n_e = 1$, and $\sqrt{m_i/m_e} = 40$. The normalized $E \times B$ shear rate is $\hat{\gamma}_E = (r/q)d[(q/r)(c/B_{unit})d\Phi^0/dr]/[c_{s0}/a] = 0.1$, and toroidal velocity shear rate is $\hat{\gamma}_\phi = -R_0 d[(u_\phi/R)/dr]/[c_{s0}/a] = (R_0 q_0 / r_0) \hat{\gamma}_E = 1.2$. $B_{unit} = B_0$, the magnetic center toroidal field, in the so called “ $s - \alpha$ ” large aspect ratio circular geometry used here, where $|\nabla r| = 1$ ($\alpha = 0$ here). (See Ref. 18 for a description of the more general Miller geometry and the effective “shaped” magnetic field B_{unit} used in GYRO.) Here and below, the “ \wedge ” mark refers to normed (dimensionless) quantity. The unit of length a is the minor radius of the separatrix, and the unit of rate is $[c_{s0}/a]$. The relative gyroradius is $\rho_* = \rho_{s0}/a = (c_{s0}/\Omega)/a = 0.0025$, where $\Omega = eB_{unit}/cm_i$. The normalized radial electric field is $\hat{E}_r^0 = -d(e\Phi^0/T_{e0})/d(r/a) = +8$ with all these values typical of a mid radius strongly rotating DIII-D (Ref. 19) L-mode plasma, except the fluid toroidal rotation $u_\phi/[c_{s0}]$ (typically ~ 0.2) is set to 0

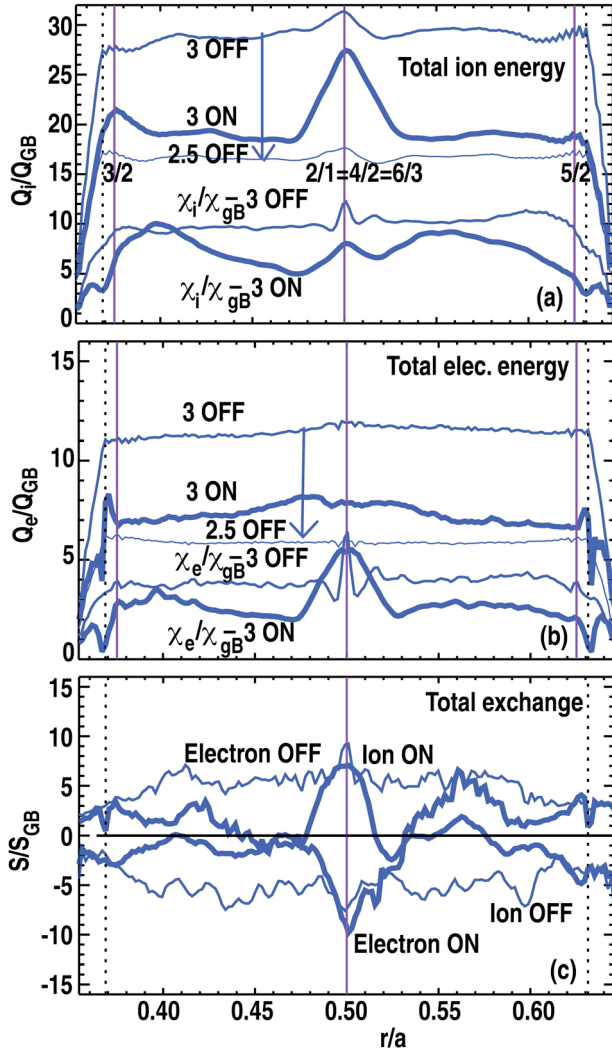


FIG. 1. (Color online) GA-std 96- n case with $\hat{E}_r^0 = +8$ (with $\hat{\gamma}_E = 0.1$, $\hat{\gamma}_\phi = 1.2$) and $\hat{A}_{||}^{ext}(r_s) = -0.006$ “ON” and “OFF” with the radial profile of ion (a) and electron (b) energy fluxes in gyroBohm units $Q_{GB} = T_{e0}n_0c_s$, and turbulent e-i exchange sources (c) in units $S_{GB} = T_{e0}n_0c_s/a$. “2.5 OFF” case has $a/L_T = 3 \Rightarrow 2.5$.

(since the Coriolis force drift has no significant effect on the case at hand).

The full-torus $\Delta n = 1$ radial slice has “zero boundary conditions” and extends over $0.35 < r/a < 0.65$ with 96 modes $n = [0, 95]$ corresponding to $k_\theta \rho_s = [0, 0.95]$. The only radial profile variation (in these “flat” profile cases) comes from $q(r) = q_0[1 + s(r - r_0)/r_0]$, and the $m/n = 6/3$ external RMP field variation comes from $\hat{A}_{||3}^{ext}(r, \theta) = -0.006 \exp[i(m - nq(r)\theta)]$ in the base case. The expected island width is $\hat{W} = 4[(\rho * /s)2\hat{A}_{||}^{ext}Rq/a]^{1/2} \sim 0.053$, close to about 5% of the minor radius (a) or 20 ion gyroradius units (ρ_s) apparent in the figures below.

We first discuss the effect of the RMP field on the energy channels in Fig. 1. Apart from the distortions within the island width located at the mid radius $r/a = r_s/a = r_0/a = 0.5$, the most striking feature is the depression of the ion [Fig. 1(a)] and the electron [Fig. 1(b)] fluxes (and diffusivities) well outside the island $|r - r_s| > W/2$ when the island is “ON” versus “OFF” at $\hat{A}_{||3}^{ext} = -0.006$ and $\hat{E}_r^0 = +8$. The RMP field even causes the turbulent electron-

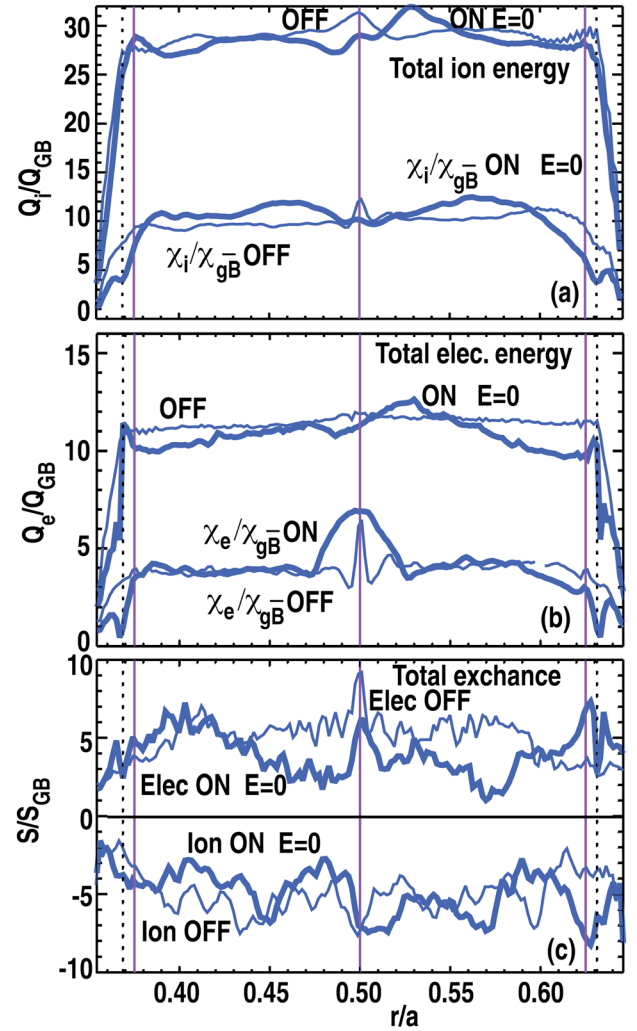


FIG. 2. (Color online) GA-std 96- n case with $\hat{E}_r^0 = 0$ otherwise same as Fig. 1 caption.

ion energy exchange²⁰ [Fig. 1(c)] to flip signs. Figure 2 shows that the outside island effects (“ON” versus “OFF” transport depressions and flip of the e-i exchange terms) vanish entirely when the imposed or background radial electric effect vanishes $\hat{E}_r^0 = 0$. (As expected, when RMP field is “OFF” there is no dependence on \hat{E}_r^0 although as well known, sufficient $E \times B$ shear $\hat{\gamma}_E$ can quench the transport.²¹) When $\hat{E}_r^0 = 0$, the ion and electron energy fluxes through the island are continuous [Figs. 2(a) and 2(b)], and the only effect of the island is the increase in the electron energy diffusivity $\chi_e = Q_e/[n_0T_e(-\partial \ln T_e/\partial r)]$ [see Fig. 2(b)] over the island due to the expected electron temperature gradient flattening inside [$\Delta(a/L_{Te}) \approx -1.5$] and steepening outside the island. The distortion (bump) in $\chi_e(r)$ [as in Fig. 1(b)] indicates a significant loss of confinement over the island and appears to be consistent with an island full width $\hat{W} \sim 5\%$. When the RMP field is “OFF,” the remaining distortion of χ_e at $q(r_0) = 2$ [see Fig. 2(b)] is due to the experimentally verified zonal flow profile corrugations in $-\partial \ln T_e/\partial r$ at low order $q(r_0) = m/n = 2/1$ rational surfaces.²² The ion energy diffusivity is only weakly affected [see Fig. 2(a)].

Figure 3 shows that RMP field causes significant distortions of the (unperturbed) FSA plasma temperature, density, and

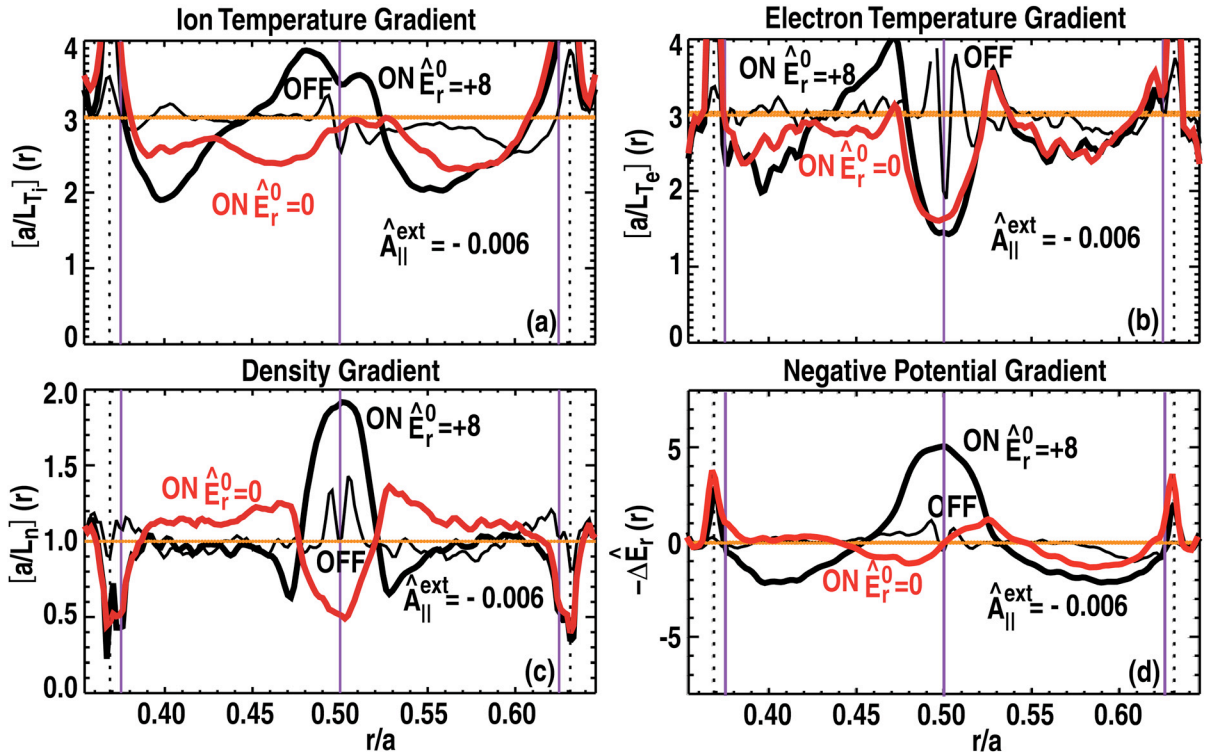


FIG. 3. (Color online) GA-std 96- n case with $\hat{E}_r^0 = +8$ (with $\hat{\gamma}_E = 0.1$, $\hat{\gamma}_\phi = 1.2$) and $\hat{A}_{||}^{ext}(r_s) = -0.006$ “ON” and “OFF” with the time and flux surface average ($n = 0$) radial profiles of total ion (a) and electron (b) temperature gradients [$^{net}[a/L_{T_i}](r)$], density gradient (c) [$^{net}[a/L_n](r)$], and gradient of perturbed potential (d) $-\hat{\Delta E}_r(r)$.

electric field profiles over the island. For $\hat{E}_r^0(r_s) = +8.0$, Fig. 3(d) shows that at the 6/3 singular surface, there is a back reaction $\hat{\Delta E}_r(r_s) \approx -5.0$ which when combined with the background gives a net $^{net}\hat{E}_r^0(r_s) = \hat{E}_r^0(r_s) + \hat{\Delta E}_r(r_s) = +3.0$. At $\hat{E}_r^0(r_s) = 0$, the back reaction vanishes; from the \hat{E}_r^0 scan, a good description of the back reaction is given by $\hat{\Delta E}_r \approx -0.6\hat{E}_r^0$. The corresponding distortion of the density is shown in Fig. 3(c) and temperature gradients in Figs. 3(a) and 3(b). The $^{net}[a/L_{n,T}](r_s) = [a/L_{n,T}]^0(r_s) + \Delta[a/L_{n,T}](r_s)$ can be roughly described by $\Delta[a/L_n](r_s) \approx 0.2[\hat{E}_r^0(r_s) - 2.5]$, $\Delta[a/L_{Te}](r_s) \approx -1.5 - 0.03\hat{E}_r^0(r_s)$, and $\Delta[a/L_{Ti}](r_s) \approx -0.5 + 0.1|\hat{E}_r^0(r_s)|$. For the $\hat{E}_r^0(r_s) = +8$ case, the electrons appear to be in radial force balance $^{net}\hat{E}_r^0(r_s) = ^{net}[a/L_n](r_s) + ^{net}[a/L_{Te}](r_s)$; however, this is purely coincidental and does not hold at other $\hat{E}_r^0(r_s)$. Neither perturbed electron $\Delta\hat{E}_r = \Delta[a/L_n] + \Delta[a/L_{Te}]$ nor ion $-\Delta\hat{E}_r = \Delta[a/L_n] + \Delta[a/L_{Ti}]$ radial force balance appear to hold for the island (although in the absence of induced islands the zonal flows are known to be in ion radial force balance²²). As described in Sec. I, the buildup of the (helical) island $\Delta\phi$ distortion that produces the $E \times B$ radial electron flow canceling the MF radial electron flow which results from a nonzero parallel electron flow (thermal forces aside) $\Delta j_{||}^e = -eD_{||}[-\nabla_{||}\Delta n + n(e/T)\nabla_{||}\Delta\phi] \neq 0$ suggesting Δn is not exactly $n(e/T)\Delta\phi$ but only close to $n(e/T)\Delta\phi$, i.e., we should not expect exact radial force balance in the electron fluid. In the RMP field “OFF” case, the remaining *profile corrugations* are much less than the RMP “ON” island distortions.

Outside the island in Fig. 3(a) indicates a significant depression of the ion temperature gradient $^{net}[a/L_{Ti}] = 3 \Rightarrow 2.5 - 2.0$ (comparing “ON” to “OFF”). There is also a significant increase in the local radial average zonal flow $E \times B$ shearing rate $]\hat{\gamma}_E^{ZF}[= 0 \Rightarrow \approx 0.2$ compared to the background $\hat{\gamma}_E = 0.1$ ($\hat{\gamma}_E^{ZF} = \rho_* \partial[\partial\delta\phi_{n=0}/\partial r]/\partial r$). The static $n = 3$ RMP field appears to be nonlinearly pumping the zonal flows, increasing the $E \times B$ shearing and perhaps more importantly decreasing the driving temperature gradients. The increase in $]\hat{\gamma}_E^{ZF}[$ and depression of $^{net}[a/L_{Ti}]$ are considerably less when $\hat{E}_r^0(r_s) = +8$ is reset to 0 (see again Fig. 2, where the outside depression of the energy flux is not significant). As a technical aside, these GYRO global slice simulations did not include the “adaptive sources,” which prevent “transport profile gradient relaxation,” which appears to be small here. (There is no evidence of this “transport” relaxation in the “OFF” case which has larger transport.)

RMP “ON” versus “OFF” transport, outside the island in particular, is compared at the same driving temperature gradients. Figure 3(c) showed no depression of the density gradient outside the island, but as noted, the depression of the temperature gradients is significant [Figs. 3(a) and 3(b)]. From Figs. 1(a) and 1(b), it is shown that RMP “OFF” simulations with reduced $[a/L_T]^0 = 3 \Rightarrow 2.5$ bring the transport outside the island to closer agreement with the RMP “ON” $[a/L_T]^0 = 3$ case. The increase in ion energy flux within the island [Fig. 1(a)] is due to the ion convection associated with the nonambipolar particle flow as discussed later.

When $\hat{E}_r^0(r_s) \neq 0$, we have no clear understanding as to why the external $n = 3$ RMP field appears to pump the $n = 0$

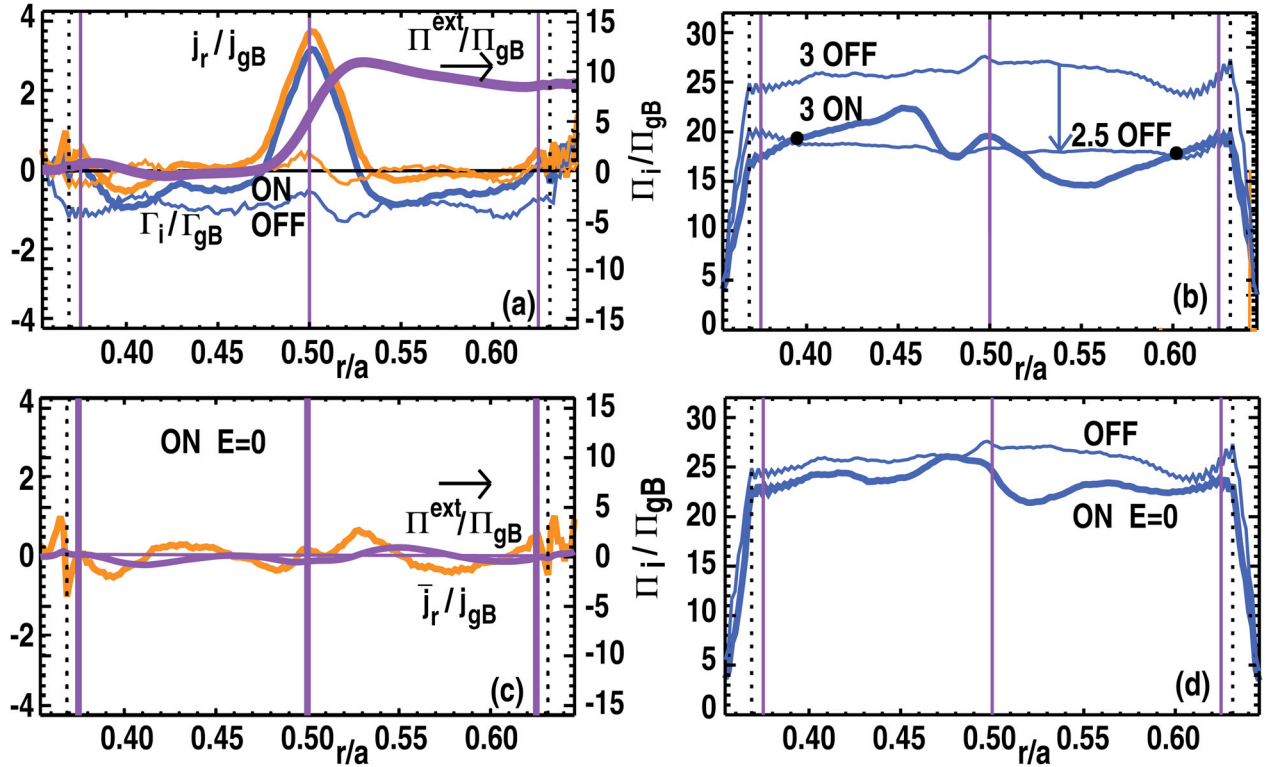


FIG. 4. (Color online) GA-std 96- n case with $\hat{E}_r = +8$ in (a) and (b) and $\hat{E}_r = 0$ in (c) and (d). $\hat{\gamma}_E = 0.1$, $\hat{\gamma}_\phi = 1.2$, and $\hat{A}_{||}^{ext}(r_s) = -0.006$ “ON” (thick lines) and “OFF” (thin lines). The time and flux surface average ($n = 0$) radial profiles of the gyrokinetic radial current flux j_r in gyroBohm units $j_{gB} = en_0 c_s \rho_s^2$ [thick yellow (or grey)] in (a) and (c). Ion particle flux Γ_i in units $\Gamma_{gB} = n_0 c_s \rho_s^2$ in (a) [thick and thin blue (or black) lines]. The externally induced integrated torque density TAM flux units Π^{ext} in (a) and (c) [very thick purple (or black) lines]. The transport TAM flux $\hat{\Pi}_i$ in (b) and (d) in units $\Pi_{gB} = am_i n_0 c_s^2 \rho_s^2$. “2.5 OFF” case has $a/L_T = 3 \Rightarrow 2.5$.

zonal flows lowering the driving (ITG) temperature gradients (outside the island) and slightly increasing the $E \times B$ shear. It is important to realize that changes in the gradients in Fig. 3 are temperature, density, and potential components of the zonal flows. However, Wilson and Conner²³ have argued that (long-thin) islands tend to stabilize (cold ion sheared slab) ITG [actually $\eta_i = (a/L_{Ti})/(a/L_n)$] modes when the Doppler rotation is not zero and *only when* modifications of the temperature and density profiles *within* the island are accounted for (see Fig. 3 of Ref. 13). Figure 3 shows that the unperturbed flux surface average $\eta_i = 3 \rightarrow 1.8$ decreases inside the island. In contrast, for the simulations here, we are more concerned with explaining the reduction in turbulence levels and transport flux levels well outside the island. As we discuss below, a similar reduction in the toroidal momentum flux (viscous or Reynolds stress) outside the island considerably complicates the discussion of net magnetic braking which combines the Reynolds stress and the Maxwell stress due to the presence of an externally induced island.

The discussion of Fig. 3 *island profile distortions* is a good place to compare and contrast with the related gyrokinetic induced island simulations of Ref. 13. In contrast to the FSA distortions with respect to the unperturbed flux surfaces here, contour plots and radial plots through the X and O points of the island are given there. Only the $\hat{E}_r^0(r) = 0$ case is considered and nonambipolar radial flows are not, otherwise we find no contradiction with our results.

Our main focus is on nonambipolar current flux and the TAM braking torque shown in Fig. 4 contrasting $\hat{E}_r = 8$ [Figs.

4(a) and 4(b)] with $\hat{E}_r^0 = 0$ [Figs. 4(c) and 4(d)]. The radial current flux $\hat{j}_r(r)$ [thick yellow (or grey) “ON” and thin yellow (or grey) “OFF”] tracks the ion flux in the RMP “ON” case [thick blue (or black) line] in Fig. 4(a). The ion flux “OFF” case [thin blue (or black) line] shows the pinched influx common to the GA-std case. Also shown is the integrated torque density (or Maxwell stress) TAM flux (thick purple line): $(\Pi^{ext}(\hat{r})/\Pi_{gB}) = 1/\hat{r} \int_0^{\hat{r}} \hat{r}' d\hat{r}' [(\hat{r}'/q(\hat{r}')/\rho_*) \hat{j}_r(\hat{r}')]^2$ which can be compared with the (viscous or Reynolds stress) TAM transport flux $(\hat{\Pi}_i/\Pi_{gB})$ in Fig. 4(b). Note that $[(\hat{r}/q)/\rho_*] = 100$ at $\hat{r} = 0.5$ for the GA-std case. On the outer side of the island, $\hat{\Pi}^{ext}(\hat{r}_s + \hat{W}/2) \sim 10$ which is comparable to the viscous transport $\hat{\Pi}_i^{“3-ON”}(\hat{r}_s + \hat{W}/2) \sim 15$ (in this particular case). (It should be noted that the TAM transport fluxes $\hat{\Pi}_i$ in Figs. 4(b) and 4(d) do not include the convection of TAM, $\hat{\Pi}_i^{conv} = \hat{\omega}_0 \hat{\Gamma}_i$. At moderate rotation $\hat{E}_r = 8$, the toroidal rotation frequency $\hat{\omega}_0 = 0.12$ for the case at hand. The $\hat{\Gamma}_i \sim -1$ exterior to the island is the usual particle pinch flux associated with the GA-std case and the extra island ion convection $\hat{\Gamma}_i(\hat{r}_s) = 3$. The small convection of TAM, $\hat{\Pi}_i^{conv}$ is negligible.)

Combining $\hat{\Pi}^{ext}(\hat{r}_s + \hat{W}/2) + \hat{\Pi}_i^{“3-ON”}(\hat{r}_s + \hat{W}/2) = 25 \sim \hat{\Pi}_i^{“3-OFF”}(\hat{r}_s + \hat{W}/2)$ at first *appears* to imply that “turning ON” the RMP induced island would not brake the toroidal rotation since no additional TAM flux *appears* to be carried away from the island. However, we believe the apparent equality is an artifact of the simulation and this interpretation is incorrect. As measured well away from island, the viscous TAM flux $\hat{\Pi}_i^{“3-ON”}(r)$ is unchanged passing through the island at 17

gyroBohm units [indicated by the dots in Fig. 4(b)]. This value (and the radial box average $\hat{\Pi}_i^{3-ON}$) is the same as the “OFF” viscous TAM flux $\hat{\Pi}_i^{2.5-OFF} \sim 17$ measured at the same “effective” average driving ion temperature gradient $a/L_{Ti} = 2.5$. Turbulent transport fluxes should always be compared at the same driving gradients. We believe the correct interpretation is that the additional (and physically relevant) island TAM flux carried away is $\hat{\Pi}^{ext}(\hat{r}_s + \hat{W}/2) \sim 10$ and the “background” viscous TAM flux passing through the island is irrelevant to the additional island TAM flux. Shoring up this argument is the fact that the dominant drive for $\hat{\Pi}_i$ is the toroidal velocity shear ($\gamma_\phi = 1.2$ in this case). When γ_ϕ and γ_E (as well as profile variation residual stress⁷) are taken to vanish, the box averages $\hat{\Pi}_i^{3-ON}$, $\hat{\Pi}_i^{3-OFF}$, and $\hat{\Pi}_i^{2.5-OFF}$ vanish, but $\hat{\Pi}^{ext}(\hat{r}_s + \hat{W}/2)$ is unchanged. Recall Fig. 1(a) showed that the background energy fluxes [\hat{Q}_i, \hat{Q}_e] “ON” versus “OFF” were also largely unchanged when compared at the same “effective” average driving ion temperature gradient $a/L_{Ti} = 2.5$.

Figures 4(c) and 4(d) show that the nonambipolar current flow gyrokinetic $\hat{j}_r(r)$ and most importantly $\hat{\Pi}^{ext}$ vanish for $\hat{E}_r^0 = 0$. The small spatially oscillating $\hat{j}_r(r)$ nonambipolar current fluxes in Fig. 4(a) when the RMP is “OFF” is spurious, since GYRO finds it more convenient to output the *gyrokinetic* fluxes derived from Eq. (7) rather than the *physical* fluxes derived from Eq. (8). [The small difference between *gyrokinetic* and *physical* fluxes is normally difficult to notice except when plotting $\hat{j}_r(r)$.] A local radial average removes this spurious nonambipolar flux which has no effect on the measurable $\hat{\Pi}^{ext}(\hat{r})$. The radial box (and unperturbed flux surface average) toroidal mode number n -spectrum from the $n = 3$ RMP induced \hat{j}_r and $\hat{\Pi}^{ext}$ is almost wholly contained within the $n = 3$ spectral component, whereas [$\hat{\Pi}_i, \hat{Q}_i, \hat{Q}_e, \hat{\Gamma}_i, \hat{\Gamma}_e, \hat{S}_{ei}$] spectra are largely unchanged from the unperturbed n -spectra which are spread over all n 's typically with peaking around $k_\theta \rho_s \sim 0.3$ (or $n \sim 32$ for the 96-mode simulation).

Unlike the simple test cases here, the focus of most of the RMP experimental work is of course at the tokamak edge

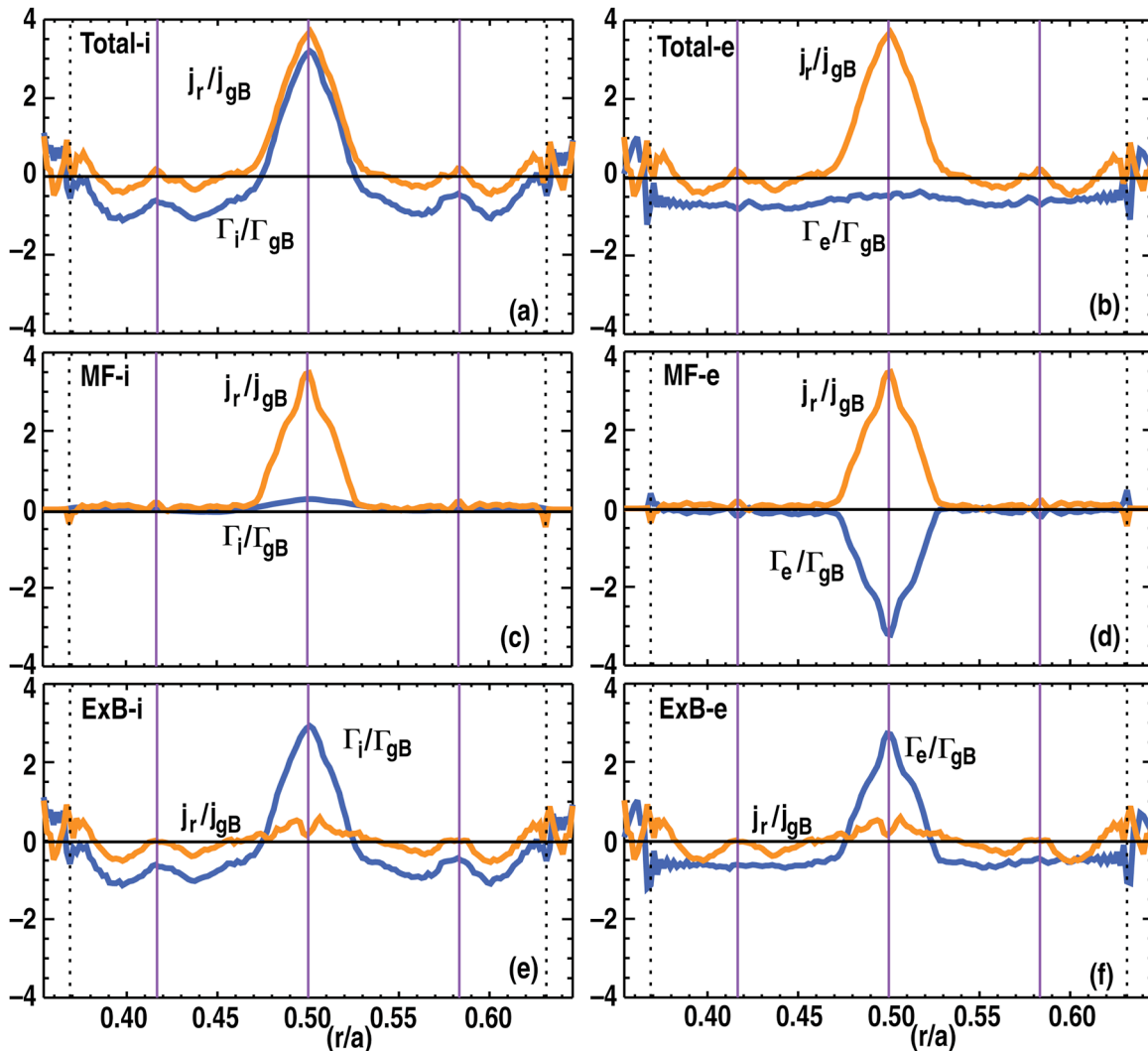


FIG. 5. (Color online) GA-std 32- n case with $\hat{E}_r^0 = +8$ and $\hat{\gamma}_E = 0$, $\hat{\gamma}_\phi = 0$, and $\hat{A}_{||}^{ext}(r_s) = -0.006$ “ON.” The time and flux surface average ($n = 0$) radial profiles of the gyrokinetic radial current flux j_r in gyroBohm units $j_{gB} = en_0 c_s \rho_s^2$ [thick yellow (or grey) lines] particle fluxes Γ in units $\Gamma_{gB} = n_0 c_s \rho_s^2$. [thick blue (or black) lines]. Total ions in (a) and electrons in (b). MF ion in (c) and electron in (d), $E \times B$ ion in (e) and electron in (f).

where the (vacuum) RMP fields are strongest and the vacuum level external field induced islands are overlapping. The norm $\hat{A}^{ext}(r) = -0.006$ is radially constant in the simulations, whereas experimentally $\hat{A}^{ext}(r)$ would fall-off from the edge like $(r_{coil}/r)^{m-1}$. Furthermore and most importantly, the actual $n = 3$ DIII-D RMP coils typically have a 50-50 mixture of co- and ctr-helicity⁴ and mixture of m 's dominated typical by $m/n = \pm 11/3$ with the resonant component close to the edge. The nonresonant (ctr-helicity) component is less screened. The GYRO simulations claim only to properly treat co-helicity resonant perturbations. Flipping the co-helicity $m/n = 6/3$ RMP treated here to ctr-helicity $m/n = -6/3$ (which produces no islands) results in three smaller and similar non-overlapping radial current peaks at $q(r) = 6/3$ at $r/a = 0.5$ as well as at $q(r) = 5/3$ and $7/3$ at $r/a \sim 0.42$ and 0.58 , respectively, and even somewhat larger net torquing than the co-helicity resonant case of Fig. 4(a). We hasten to say, however, that all these peaks and the large ctr-helicity nonresonant torquing are very likely unphysical and a spurious result from the high- n perpendicular derivative approximation used in GYRO. As we explained below, Eq. (16) in Sec. II, the approximation is less of a worry for resonant or co-helicity external RMP fields (There is no significant nonresonant torquing at $q(r) = 5/3$ and $7/3$ in the co-helicity case.) The long planned GYRO reformulation replacing the $\nabla_y \Rightarrow inq/r$ “ballooning mode” operator with the proper $\nabla_y \Rightarrow [(inq - \partial_\theta)]/r$ is needed to verify any significant level of ctr-helicity nonresonant torquing. This is left to future work as is more experimentally realistic RMP simulations.

IV. DEPENDENCE OF THE NONAMBIPOLAR CURRENT AND MAGNETIC BRAKING TORQUE ON RADIAL ELECTRIC FIELD, ISLAND WIDTH, AND INTENSITY OF THE HIGH- N TURBULENCE

To determine the scaling of the $n = 3$ RMP induced nonambipolar current \hat{j}_r (and corresponding island TAM flux $\hat{\Pi}^{ext}$) with respect to \hat{E}_r^0 , island width \hat{W} , and the intensity of the high- n turbulence I , we reduced the full torus $\Delta n = 1$ 96-mode simulations to much less expensive partial torus $\Delta n = 3$ radial slice with $32-n$ modes spanning the same $k_\theta \rho_s = [0, 0.95]$ high- n ITG/TEM turbulence. Continuing the GA-std case electrostatic collisionless GYRO simulations ($\beta_e = 0$, $\delta \hat{A}_\parallel = 0$, $\nu_{ei} = 0$), the irrelevant $E \times B$ velocity shear was reduced to zero: $\hat{\gamma}_E = 0.1 \Rightarrow 0$. The difference between full and partial torus ($\Delta n = 1 \Rightarrow 3$) is not significant: transport flows are reduced by about 10%. The neglect of $E \times B$ shear stabilization increased the transport flows by about 30%. As noted above, the additional zeroing of $\hat{\gamma}_\phi = 1.2 \Rightarrow 0$ reduces the box average $\hat{\Pi}_i$ to zero, but otherwise $\hat{\gamma}_\phi$ is not relevant to the problem at hand. \hat{j}_r^{peak} and $\hat{\Pi}^{ext}$ are (nearly) unchanged.

First, we have decomposed the total nonambipolar radial current flux into $E \times B$ and magnetic flutter (MF) as well as ion and electron parts in Fig. 5. It is clear from Figs. 5(a) and 5(b) that the total nonambipolar radial current flux is carried almost entirely by the ions. This results because the electrons move so quickly along the (parallel) field lines of the island

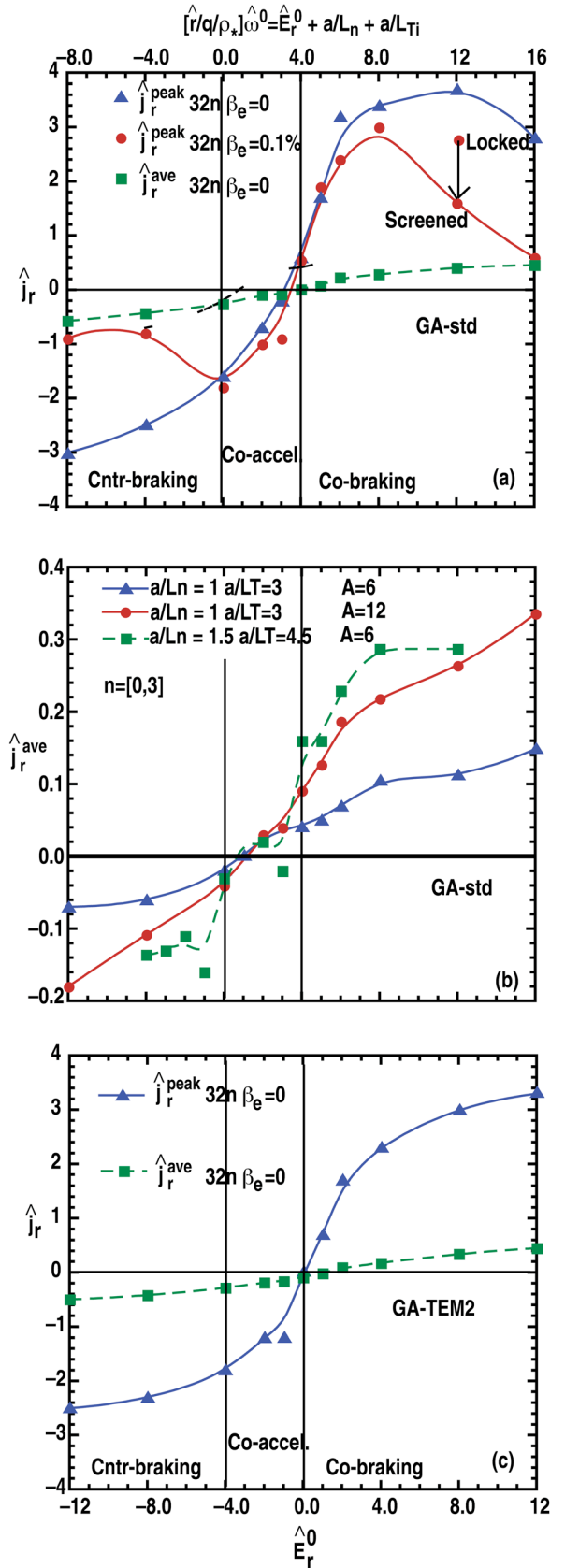


FIG. 6. (Color online) GA-std case at $\hat{\gamma}_E = 0$, $\hat{\gamma}_\phi = 0$, and $\hat{A}_\parallel^{ext}(r_s) = -0.006$ “ON” with normed peak \hat{j}_r^{peak} and box average \hat{j}_r^{ave} current flux versus radial electric field \hat{E}_r^0 (lower axis) and toroidal rotation frequency $\hat{\omega}^0$ for 32- n modes in (a) and 2- n modes “bare” island in (b) with additional $\hat{A}_\parallel^{ext}(r_s) = -0.012$ and 3/2 larger $[a/L_n, a/L_T]$. (c) repeats (a) with GA-std case replaced by GA-TEM2 case ($[a/L_n, a/L_T] = [1, 3] \Rightarrow [3, 1]$), so ion fluid rest point is unchanged.

that an $m/n = 6/3$ potential is set up within the island to hold them back (see example in Ref. 13). In contrast the ion moves much more slowly along parallel field lines. Comparing Figs. 5(d) and 5(f), the resulting $m/n = 6/3 E \times B$ radial particle transport of the electrons [Fig. 5(f)] is almost completely cancelled by their MF transport [Fig. 5(d)]. However, since $E \times B$ transport is intrinsically ambipolar [with no significant $E \times B$ current flux in Figs. 5(e) and 5(f)] and the ions have very little MF transport particle flux [Fig. 5(c)], we can say the matching $E \times B$ radial particle transport of the ions [Fig. 5(e)] carried the nonambipolar current flux through the island. Alternatively, we can say that the MF electron transport carries all the nonambipolar radial current, since the ion and electron $E \times B$ radial transport cancel [Figs. 5(e) and 5(f)]. This is consistent with the observation that the island radial current is carried exclusively in the $n=3$ harmonic and that there must be a time average $m/n = 6/3 \delta\hat{\phi}$ perturbed potential set-up to match the static $m/n = 6/3 \Delta\hat{A}_{\parallel}^{ext}$. The “bump” in the ion particle flux over the island in Fig. 5(a) [missing from the electron flux in Fig. 5(b)] implies that the “bump” in the ion energy flux in Fig. 1(a) [missing from the electron flux in Fig. 1(b)] is due to energy convection $[(3/2)T_i\Gamma_i]$. We should caution that this description applies to a large and isolated island. (Some very preliminary cold collisional edge simulations with many moderately high- n small and overlapping islands over a wide radial regions, possibly like those induced by external field errors, show the electrons carry all the nonambipolar radial current over a wide region by MF and there is no $E \times B$ current in the ions: the induced $\Delta\phi$ is apparently “shorted out” by the island overlap.)

Figure 6(a) shows the peak or the radial current flux $\hat{j}_r(\hat{r}_s)$ versus the radial electric field \hat{E}_r^0 (lower axis) and the corresponding toroidal rotation frequency $\hat{\omega}^0$ (upper axis) assuming radial force balance without poloidal rotation. From Eq. (15) $[\hat{r}/q/\rho_*]\hat{\omega}^0 = \hat{E}_r^0 + a/L_{Ti} + a/L_n$ with $\hat{\omega}^0 > 0$ (< 0) co- (ctr-) current fluid toroidal rotation. Up to large rotation \hat{E}_r^0 , $\hat{j}_r(\hat{r}_s)$ is described by a simple constant and positive mobility $\mu; \hat{j}_r(\hat{r}_s) = en_0\mu(r_s)E_r^0(r_s)$ consistent with magnetic braking torque flux Π_i^{ext} . Most importantly $\hat{j}_r(\hat{r}_s)$ [the radial box average $\hat{j}_r(r)$] and hence the magnetic braking torque flux Π_i^{ext} vanishes at $\hat{E}_r^0 \sim 0$ where $\hat{\omega}^0 = +4\rho_*(q/\hat{r})$ has a small diamagnetic level co-current. At large co-current rotation $\hat{\omega}^0 > +4\rho_*(q/\hat{r})$ and ctr-current $\hat{\omega}^0 < 0$ the island brakes the rotation, but at very small co-rotation $0 \leq \hat{\omega}^0 < +4\rho_*(q/\hat{r})$ there is an *island residual stress* or *magnetic co-acceleration*. It has not escaped our notice that this is similar to the (RMP “OFF”) *residual stress* driven mostly co-current diamagnetic level “spontaneous rotation” [7]. It suggests toroidal field errors may contribute. (The finite- β RMP field screening and mode locking [red line in Fig. 6(a)] are discussed in Sec. V below.) Fig. 6(b) makes a similar plot of the radial box average $\hat{j}_r(r)$ for the “bare” island 2-mode $n = [0, 3]$. Contrasting with the high- n turbulence driven island transport in Fig. 6(a) (with $n = [0, 3, 6, 9, \dots, 93]$) the “bare” island torque in Fig. 6(b) is about 5-fold less: at $\hat{E}_r^0 = 12$ and $\hat{A}_{\parallel}^{ext} = -0.006$ with same gradients, the radial box average $\hat{j}_r(r)$ is 0.5 for the turbulent

island Fig. 6(a) and 0.1 for the “bare” island in Fig 6(b). The null torque is closer to $\hat{\omega}^0 \sim 0$ rather than $\hat{E}_r^0 \sim 0$. Thus the *island residual stress* is due to the high- n turbulence. Fig. 6(c) repeats the ITG mode dominated GA-std $\beta_e = 0$ case of Fig. 6(a) but with the TEM dominated GA-TEM2 case with $([a/L_n, a/L_T] = [1, 3] \Rightarrow [3, 1])$ so ion fluid rest point $\hat{E}_r^0 = -4$ is unchanged. Again the null torque is close to $\hat{E}_r^0 \sim 0$. [In the GA-std (GA-TEM2) case the null point might lean a little toward $\hat{E}_r^0 = -1.0(+1.0)$ but certainly not close to the ion rest point $\hat{E}_r^0 = -4$].

The null torque at $\hat{E}_r^0 = 0$ is significant in the context of intrinsic tearing modes, since $\hat{E}_r^0 = 0$ determines the “natural” (unforced) rotation frequency of the island. This frequency is important since it determines the sign of the polarization current, which is believed to provide the threshold against excitation of the NTM.

It is useful to ask if anything like *island residual stress* has been seen before. The closest comparison is with the work by Waelbroeck *et al.*,¹⁴ which treated the “effect of electrostatic turbulence on magnetic islands.” Reference 14 presented simple 2D ($[xyz] \partial_z = 0$) *sheared slab* simulations of a cold ion density gradient driven two-fluid *collisional* drift wave Hasagawa-Wakatani²⁴ model generalized to include small stationary islands with $w = [0.5, 1.5, 2.9, 4.1]\rho_s$ compared to the $w = 20\rho_s$ island here. The stationary island was embedded in the cold ion fluid $E \times B$ streaming in the (minus) y -direction with the equivalence $u \Leftrightarrow \hat{E}_r^0$ with $n' = -1 \Leftrightarrow a/L_n = 1$, so the ion fluid rest point in the $0 \leq u \leq 1$ scan is at $u = 0$. [Since ions are cold, the equivalent toroidal rotation frequency is $\hat{\omega}^0 = \hat{E}_r^0 \rho_*(q/\hat{r})$ (rather than as in Fig. 6) and $u = 0(1) \Leftrightarrow \hat{E}_r^0 = 0(1)$]. $u = 1$ corresponds to the ion $E \times B$ velocity equal and opposite to the electron diamagnetic velocity so the electron fluid (external to the island)

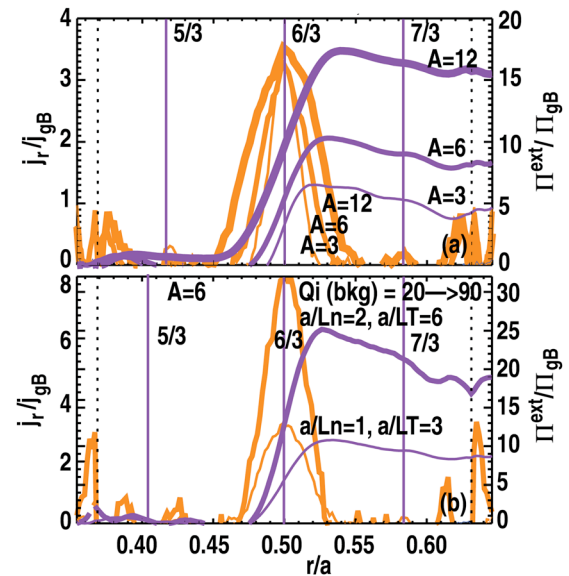


FIG. 7. (Color online) GA-std 32- n case with $\hat{E}_r^0 = +8$ and $\hat{\gamma}_E = 0$, $\hat{\gamma}_\phi = 0$ radial profiles of normed radial current flux j_r and island torque flux Π^{ext} scanning $\hat{A}_{\parallel}^{ext}(r_s) = [-0.003, -0.006, -0.012]$ in (a) and doubling $[a/L_n, a/L_T] = [1, 3] \Rightarrow [2, 6]$ with $\hat{A}_{\parallel}^{ext}(r_s) = -0.006$ in (b). $j_{GB} = en_0c_s\rho_*^2$ and $\Pi_{GB} = am_in_0c_s^2\rho_*^2$.

is at rest with respect to the stationary island; $u = 1 \Rightarrow n_e = e\phi/T_e$ and the electrons are adiabatic. Hence, the electrons can carry no radial current and $u = 1$ is said to be a “universal” null torque point [$F_y = 0 \iff j_r^{ave} = 0$]. Reference 14 found other stable null torque points near $u = 0.8$ for the smallest islands $w = [0.5, 1.5]\rho_s$ and near ion rest at $u \sim 0.15$ for the largest island $w = 4.1\rho_s$ with multiple null points $u \sim [0.4, 0.8]$ for intermediate size islands $w = 2.9\rho_s$. In contrast to the cases here, the torque F_y and null torque points for the “laminar” [suppressed turbulence similar to the “bare” islands in Fig. 6(b)] and “turbulent” cases were almost indistinguishable. Null torque points with $u > 0$, means that an ion (center of mass) fluid at rest with respect to a stationary island would be accelerated in the equivalent of the co-current direction to one of the stable null torque points. The co-current ion acceleration from rest to small diamagnetic level rotation is entirely similar to that in Figs. 6(a) and 6(c). This is certainly qualified as *island residual stress*, although the underlying physical model is in contrast with the *collisionless* and *toroidal* ITG/TEM gyrokinetic simulations here.

Figure 7(a) shows that although the peak nonambipolar radial current is not very sensitive to the external field strength $\hat{A}^{ext}(r_s)$, the increasing width of the island $\hat{W} \propto [\hat{A}^{ext}(r_s)]^{1/2}$ means that the radially integrated torque (density) or island momentum flux is proportional to the island width: $\hat{\Pi}^{ext}(\hat{r} + \hat{W}/2) \propto \hat{W}$. From the earlier observation that the “bare” island has comparatively little braking torque, we can expect the island momentum flux to increase significantly with the intensity I of the high- n turbulence. By doubling the driving gradients $[a/L_n, a/L_T] = [1, 3] \Rightarrow [2, 6]$, the time average RMS $I = \sum_{n \neq 0} |\delta\phi_n|^2$ increases 4-fold and as shown in Fig. 7(b) $\hat{\Pi}^{ext}(\hat{r} + \hat{W}/2) \propto \hat{W}$ (and $\hat{j}_r(\hat{r}_s)$) increased somewhat more than 2-fold. We can conclude that $\hat{\Pi}^{ext}(\hat{r} + \hat{W}/2) \propto \sqrt{I}$. This is consistent with Eq. (7). Since $\delta A_{||} = 0$ here and $\Delta A_{||}^{ext}$ is fixed, the MF electron radial current flux in the $n = 3$ channel is $^{MF}j_r^e = -\int dv^3 \langle \nabla r | (c/B) \{ -\nabla_y \langle -v_{||} / c \Delta A_{||}^{ext} \} \delta g \rangle_{fsa} \propto \delta g$ which scales with the high- n nonlinear drive amplitude: $|\delta\phi|^{RMS} = \sqrt{I}$. We should note, however, that the formula does not explain why j_r^{peak} appears to be independent of $\Delta A_{||}^{ext}$. Recall from Fig. 5 that the MF electron radial island flux is completely cancelled by the electron $E \times B$ which is equal to the ion $E \times B$ flux through the island. By increasing the electron-ion collisionality $\hat{\nu} = \nu_{ei}/[c_s/a] = 0 \Rightarrow 0.2$, the \sqrt{I} dropped by 1.5-fold as did $\hat{\Pi}^{ext}(\hat{r} + \hat{W}/2) \propto \sqrt{I}$; hence, it is difficult to isolate any strong effect of collisionality apart from the dependence on the high- n turbulence intensity. In the ion gyroBohm units used here, there is not much dependence on the inverse root of the electron mass $\mu = \sqrt{m_i/m_e} = 40(H) \Rightarrow 60(D)$. Since the electron parallel field motion is so fast, once the electron $E \times B$ and MF radial current flow through the island nearly cancel [Figs. 5(d) and 5(f)], there is not much room left for more cancellation. In addition, the high- n electrostatic turbulence is not very sensitive to μ .

It is useful to compare the turbulent island radial current relaxation (or essentially the rotation braking) rate with the

global ion energy confinement loss rate. The ions carry the radial current and the excess charge which must be shed from inner to outer side of the island to reduce the radial electric field. From Fig. 4(a), the island ion (or charge) density relaxation rate is $1/\tau_{isl}^n = -\partial n_i / \partial t / n_i = 1/V' \partial [V' \Gamma_i] / \partial r / n_i \sim 3/(0.03) \Rightarrow 100[c_s/a]\rho_*^2$. Using $\rho_* = 0.0025$, this corresponds to a relaxation time of $1600[a/c_s]$, which is much longer than the typical turbulence time averaging window $100[a/c_s]$ which provides the “instantaneous” current fluxes at “fixed” control \hat{E}_r^0 . (Saturated nonlinear stationary states are obtained after $50 - 100[a/c_s]$ and the typical simulations here are less than $300[a/c_s]$.) From Fig. 1(a), the global ion energy confinement loss rate (outside the island) is $1/\tau_{glob}^{Ei} = -\partial [3/2n_i T_i] / \partial t / [3/2n_i T_i] = 1/V' \partial [V' Q_i] / \partial r / [3/2n_i T_i] \sim 20/[3/2] \Rightarrow 13[c_s/a]\rho_*^2$ so the *initial* island braking rate for the $\hat{E}_r^0 = +8$, $\hat{A}^{ext} = -0.006$ case is 8-fold faster. [From the increase of the island torque flux across the island $\Delta \Pi^{ext} / \Delta r = 10/0.06 \Rightarrow 166[c_s/a]\rho_*^2$ in Fig. 4(a) and the TAM continuity Eq. (14), we find the fall rate of \hat{E}_r^0 (and hence the toroidal rotation using Eq. (15)) consistent with the $1/\tau_{isl}^n$ above.] Since $\hat{\Pi}^{ext}$ (and \hat{j}_r) scales like $\hat{E}_r^0 \sqrt{I}$ and \hat{Q}_i like I , the turbulence intensity, $[1/\tau_{isl}^n] / [1/\tau_{glob}^{Ei}] \propto \hat{E}_r^0 / \sqrt{I}$ which means the island braking rate relative to the global ion energy loss rate slows as the rotation falls, but it is also faster for weaker turbulence levels. The GA-std case core effective energy diffusivity $\chi_{eff} = (c + \chi_e) / 2 \sim 7\chi_{GB}$ [Figs. 1(a) and 1(b)] is about 7-fold larger than the well studied^{7,25} 101391.2700 DIII-D moderately rotating L-mode, so 8-fold faster braking rate compare to global energy loss rate $[1/\tau_{isl}^n] / [1/\tau_{glob}^{Ei}]$ above becomes 21-fold faster at experimental turbulence levels.

At this point, it is useful to compare and contrast the non-ambipolar radial current flux (and torque) from an externally induced isolated island to that from an externally induced region of overlapping islands and spatially stochastic (static) magnetic field lines. Replacing the single helicity $m/n = 6/3$ external field [see Eq. (16)] used in Figs. 1–7 with a multiple helicity field populating all m 's and n 's equally (with reduced amplitudes) makes a crude model of external error fields from a toroidal field coil lead localized at $[\theta, \phi] = [0, 0]$ (ignoring the physical penetration fall-off at higher m 's and n 's). A good description of the radial current flow is provided by $j_r^{stoc} = \hat{\sigma}^{stoc}(\hat{E}_r^0 - \hat{E}_r^{null})$. The current flow is spread equally over the whole stochastic field simulation region. Unlike the isolated island case where $j_r^{peak} = \hat{\sigma}^{peak} \hat{E}_r^0$ with $\hat{\sigma}^{peak}$ independent of the ΔB_r^{ext} strength, $\hat{\sigma}^{stoc} \propto [\Delta B_r^{ext}]^{1.7-1.9}$ close to the expected $\hat{\sigma}^{stoc} \propto [\Delta B_r^{ext}]^2$, expected of intrinsic “magnetic flutter” transport. The electrons carry nearly all the current with little or no induced $E \times B$ ion current; essentially the electrons (traveling along stochastic field lines) short out the whole region and the back reaction $\Delta \hat{E}_r \propto -(\hat{E}_r^0 - \hat{E}_r^{null})$ is spread equally throughout. The null electric field $\hat{E}_r^{null} \sim 2$ (for the GA-std case with $[a/L_n]^0 = 1$ and $[a/L_T]^0 = 3$) which is closer to the expected “electron root” (or “rest”), i.e., 4. The caveat on the use of the high- n ballooning mode derivative operator [see Eq. (16)] is not to be ignored here.

V. FINITE-BETA ELECTROMAGNETIC GYROKINETIC SIMULATIONS WITH SCREENING OF THE EXTERNAL MAGNETIC FIELD PERTURBATIONS WITH STRONG ROTATION

At finite- β , the plasma is diamagnetic and tends to “screen out” or suppress external field perturbations. The suppression results from parallel field currents that start to flow in the plasma generating an $n = 3$ positive $\delta\hat{A}_{||3}(r_s)$ to at least partially cancel the negative (in this case) $\Delta\hat{A}_{||3}(r_s)$. The island width [and island torque flux $\hat{\Pi}^{ext}(\hat{r} + \hat{W}/2)$] is of course proportional to the net perturbation: $\hat{W} \propto \sqrt{|\Delta\hat{A}_{||3}(r_s) + \delta\hat{A}_{||3}(r_s)|}$. The mechanism responsible for the suppression depends on the operational scenario. In RMP experiments, the field is ramped up relatively slow, so that the plasma currents effectively adjust instantaneously (i.e., on the Alfvén time) to suppress island growth. It is not really possible to treat the screening and the slower magnetic breaking process dynamically with the “flat” profile radial slice and transport time scale separated “delta- r ” fixed in time \hat{E}_r^0 simulations presented here. The screening “process” is almost instantaneous and operates throughout the braking process in which the initial (near island) \hat{E}_r^0 falls to zero (and null island torque flux), if (as we show) the initial \hat{E}_r^0 is not large enough to fully screen the RMP field. A so-called “full-f-full-field” electromagnetic simulation with boundary conditions on $\delta\hat{A}_{||3}(r)$ extended to the plasma edge (or possibly to the RMP coils) and run on transport time scales is likely needed.

The finite- $\beta_e = 0.1\%$ simulation in Fig. 8 can only be taken as an illustration of the screening. (Note that the MHD critical beta for the GA-std case is $\beta_e = 0.72\%$ and we have chosen a low beta to stay away from the subcritical beta²⁶ at $\beta_e \sim 0.3\%$.) Figure 8(a) shows a time trace of the unlocking and screening process in three phases. Quickly after the $t = 0$ start-up, the island is locked (first phase) to the lab frame where the vacuum RMP field is stationary but pulled by viscous drag from the plasma rotation to about $\pi/4$ out of phase from the vacuum island. (Note that $\pi/4$ is the critical value of unlocking predicted by MHD theory.⁹) Due to the phase offset, the effectiveness of the RMP field drive is reduced and the locked island has a width about $\sqrt{2}$ times smaller than the vacuum island. At $\hat{t} \sim 350$ island becomes unlocked and starts rotating (second phase) at $n = 3$ times the toroidal rotation frequency $\hat{\omega}_0$ while shrinking in size. The shrinking or healing of the island is caused by the fact that the rotating island experiences the RMP field as an alternating field with nearly vanishing average. In the third and final phases, the 5/6-th of the external field is screened away and the remaining island is quite small. Figure 8(b) shows the expected peaking at the resonant surface and the artificially imposed zero boundary conditions on $\delta\hat{A}_{||3}(r)$ at the radial slice boundary. In the screened $\hat{E}_r^0(r_s) = 8$ case, the electron temperature gradient [not shown] has only the low order singular surface “profile corrugation” with no clear evidence of an island flattening as in the $\beta_e = 0\%$ case of Fig. 3(b). Figure 8(c) shows that the amount of screening depends on the initial (time fixed here) $\hat{E}_r^0(r_s)$. For

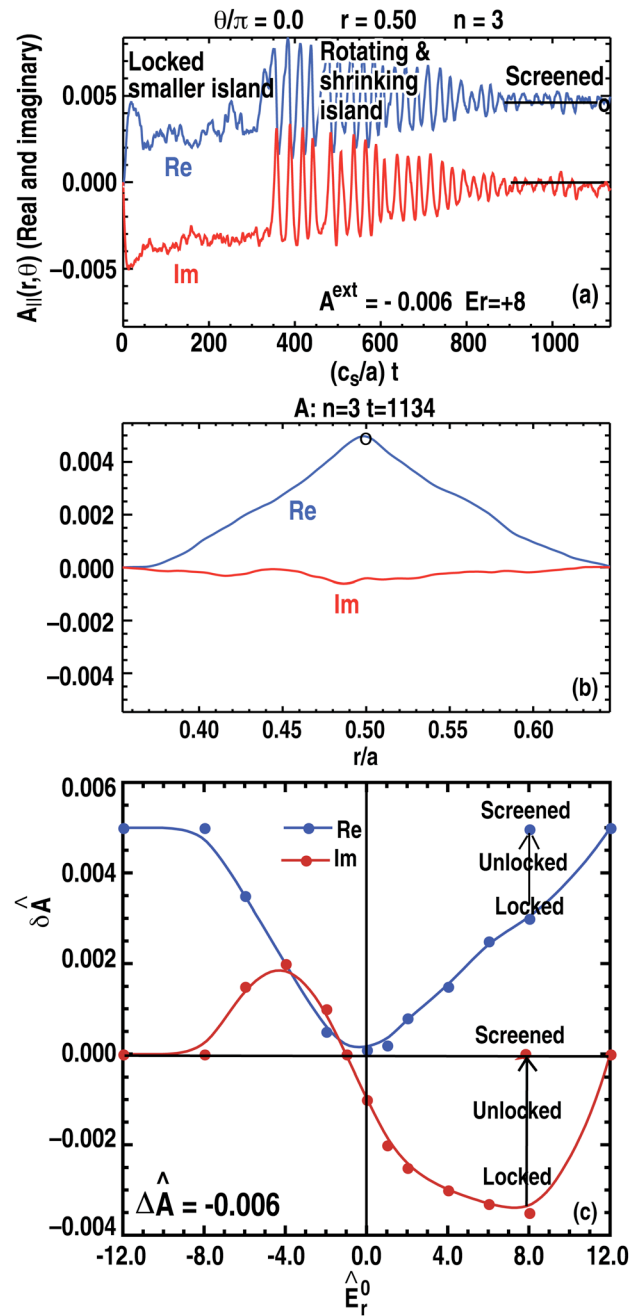


FIG. 8. (Color online) $\beta_e = 0.1\%$ GA-std 32- n case with $\hat{E}_r^0 = +8$ and $\hat{\gamma}_E = 0$, $\hat{\gamma}_\phi = 0$, and $\hat{A}_{||}^{ext}(r_s) = -0.006$ with the $n = 3$ screening field $\hat{A}_{||3}(r_s)$ versus time in (a), $\hat{A}_{||3}(r)$ versus radius after “lock” in (b), and $\hat{A}_{||3}(r_s)$ versus \hat{E}_r^0 in (c).

$-4 \leq \hat{E}_r^0(r_s) \leq +4$, the little screening and the drag phase shift are much less than $\pi/4$, the critical value for unlocking and significant screening. It appears that the unlocking and complete screening (with the net island width \hat{W} shrinking to zero) only occurs at rather large $\hat{E}_r^0(r_s)$ beyond some critical $|\hat{E}_r^0(r_s)|$ (say > 6 suggested by the figure). This is consistent with the $\beta_e = 0.1\%$ simulation of the peak island current [Fig. 6(a)] and net island torque flux shown in Fig. 9 decreasing to small levels at large $|\hat{E}_r^0(r_s)|$. Figures 8(c) and 6(a) suggest that if the RMP is “switched ON” at less than the critical $|\hat{E}_r^0(r_s)|$, not much

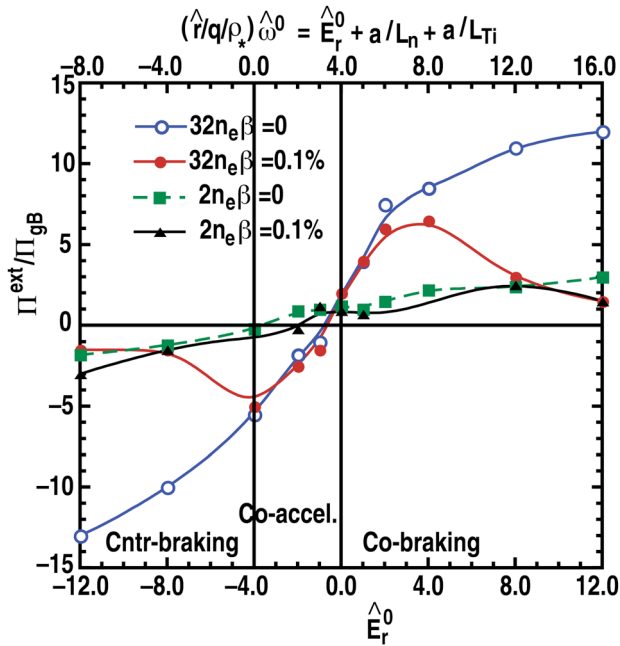


FIG. 9. (Color online) GA-std 32n and 2n (bare island) cases at $\beta_e = 0\%$ and $\beta_e = 0.1\%$ scanning $\hat{E}_r^0 = -12 \Rightarrow +12$ with $\hat{\gamma}_E = 0$, $\hat{\gamma}_\phi = 0$, and $\hat{A}_{||}^{\text{ext}}(r_s) = -0.006$ screened island torque flux $\hat{\Pi}^{\text{ext}}$, where $\hat{\Pi}_{\text{GB}} = am_i n_0 c_s^2 \rho_s^2$.

screening occurs and the island survives with the nearly initial “vacuum” width $\hat{W}_{\text{vac}} \propto \sqrt{|\Delta \hat{A}_{||3}^{\text{ext}}(r_s)|}$ at the end of the magnetic braking. The almost complete screening of the external perturbation at sufficiently large rotation and the diminution of screening at low rotation with sufficiently large vacuum island (as well as the critical drag phase shift $\pi/4$) is well known from earlier work.^{9–11} Of course, if the intrinsic tearing mode is unstable ($\Delta' > 0$), the “shielding factor” ($\hat{W}^2/\hat{W}_{\text{vac}}^2$) can exceed 1 and the vacuum island grows at sufficiently low rotation [see Ref. 27 Fig. 3]. [There is no current gradient drive (“kink term”) in the GYRO simulations here and effectively $\Delta' = 0$].

Figure 9 summarizes the screened $\beta_e = 1\%$ (compared to unscreened $\beta_e = 0\%$) island torque flux $\hat{\Pi}^{\text{ext}}$ versus $\hat{E}_r^0(r_s)$ (and toroidal rotation) for the turbulent and bare islands. The nearly complete screening at high rotation is not apparent in the bare island case where the torque flux persists. This may be due to the lack of turbulent viscosity which comes from the $E \times B$ ion motion of the high- n modes and connects the

inside island fluid to the outside. The plasma rotation is not able to drag the island past the critical phase shift to unlock it, so screening occurs.

ACKNOWLEDGMENTS

This work was supported by the U.S. Department of Energy under GA-Grant No. DE-FG02-95ER54309 and IFS Grant No DE-FG02-04ER54742. We wish to thank Dr. Todd Evans for various discussions and reviewing this paper.

- ¹J. Candy and R. E. Waltz, *J. Comp. Phys.* **186**, 545 (2003); *Phys. Rev. Lett.* **91**, 045001 (2003).
- ²R. E. Waltz, G. M. Staebler, J. Candy, and F. L. Hinton, *Phys. Plasmas* **14**, 122507 (2007); *errata* **16**, 079902 (2009).
- ³F. L. Waelbroeck, *Nucl. Fusion* **49**, 104025 (2009).
- ⁴T. E. Evans, R. A. Moyer, P. R. Thomas, J. G. Watkins, T. H. Osborne, J. A. Boedo, E. J. Doyle, M. E. Fenstermacher, K. H. Finken, R. J. Groebner, M. Groth, J. H. Harris, R. J. La Haye, C. J. Lasnier, S. Masuzaki, N. Ohyaabu, D. G. Pretty, T. L. Rhodes, H. Reimerdes, D. L. Rudakov, M. J. Schaffer, G. Wang, and L. Zeng, *Phys. Rev. Lett.* **92**, 235003 (2004); *Nucl. Fusion* **45**, 595 (2005).
- ⁵A. H. Boozer, *Rev. Mod. Phys.* **76**, 1071 (2004).
- ⁶A. H. Boozer, *Phys. Plasmas* **16**, 052505 (2009).
- ⁷R. E. Waltz, G. M. Staebler, and W. M. Solomon, *Phys. Plasmas* **18**, 042504 (2011).
- ⁸A. J. Cole, C. C. Hegna, and J. D. Callen, *Phys. Rev. Lett.* **99**, 065001 (2007); *Phys. Plasmas* **15**, 056102 (2008).
- ⁹R. Fitzpatrick, *Nucl. Fusion* **33**, 1049 (1993).
- ¹⁰R. Fitzpatrick, *Phys. Plasmas* **5**, 3325 (1998).
- ¹¹F. Militello and F. L. Waelbroeck, *Nucl. Fusion* **49**, 065018 (2009).
- ¹²E. Poli, A. Bottino, and A. G. Peeters, *Nucl. Fusion* **49**, 075010 (2009).
- ¹³W. A. Hornsby, A. G. Peeters, A. P. Snodin, F. J. Casson, Y. Camenen, G. Szepesi, M. Siccino, and E. Poli, *Phys. Plasmas* **17**, 092301 (2010).
- ¹⁴F. L. Waelbroeck, F. Militello, R. Fitzpatrick, and W. Horton, *Plasma Phys. Controlled Fusion* **51**, 015015 (2009).
- ¹⁵T. M. Antonsen and B. Lane, *Phys. Fluids* **23**, 1205 (1980).
- ¹⁶E. A. Freeman and L. Chen, *Phys. Fluids* **25**, 502 (1982).
- ¹⁷R. E. Waltz, *Phys. Fluids* **23**, 1269 (1982).
- ¹⁸R. E. Waltz and R. L. Miller, *Phys. Plasmas* **6**, 4265 (1999).
- ¹⁹M. A. Mahdavi and J. L. Luxon, *Fusion Sci. Technol.* **48**, 2 (2005).
- ²⁰R. E. Waltz and G. M. Staebler, *Phys. Plasmas* **15**, 014505 (2008).
- ²¹R. E. Waltz, G. D. Kerbel, J. Milovich, and G. W. Hammett, *Phys. Plasmas* **2**, 2408 (1995); **1**, 2229 (1994).
- ²²R. E. Waltz, M. E. Austin, K. H. Burrell, and J. Candy, *Phys. Plasmas* **13**, 052301 (2006).
- ²³H. R. Wilson and J. W. Connor, *Plasma Phys. Controlled Fusion* **51**, 115007 (2009).
- ²⁴A. Hasegawa and M. Wakatani, *Phys. Rev. Lett.* **50**, 682 (1983).
- ²⁵R. E. Waltz, J. Candy, and C. C. Petty, *Phys. Plasmas* **13**, 072304 (2006).
- ²⁶R. E. Waltz, *Phys. Plasmas* **17**, 072501 (2010).
- ²⁷F. Militello and F. L. Waelbroeck, *Nucl. Fusion* **49**, 065018 (2009).